RECURRENT HOLOCENE PALEOSEISMICITY AND ASSOCIATED LAND / SEA LEVEL CHANGES IN THE GREATER ANCHORAGE AREA

Ian Shennan, Sarah Hamilton and Antony Long

External grant award # 03HQGR0101

Investigators:
Ian Shennan, Sarah Hamilton, Ben Horton, Antony Long, John Mulholland, Catriona Noble and Yongqiang Zong
Sea Level Research Unit, Department of Geography, University of Durham, Durham, DH1 3LE, UK
and
Rod Combellick
Alaska Division of Geological and Geophysical Surveys, Fairbanks, Alaska, USA

Telephone +44 191 334 1934
Fax +44 191 334 1801
Email ian.shennan@durham.ac.uk
URL http://www.geography.dur.ac.uk

Start date: 1st May 2003
End date: 30th October 2004

Program Element II: Research on Earthquake Occurrence and Effects

Key Words: Paleoseismology; Surface Deformation; Neotectonics; Regional Seismic Hazards

Research supported by the U.S. Geological Survey (USGS), Department of the Interior, under USGS award number 03HQGR0101. The views and conclusions contained in this document are those of the authors and should not be interpreted as necessarily representing the official policies, either expressed or implied, of the U.S. Government.

© I Shennan, S L Hamilton & A J Long, 2004

RECURRENT HOLOCENE PALEOSEISMICITY AND ASSOCIATED LAND / SEA LEVEL CHANGES IN THE GREATER ANCHORAGE AREA

Ian Shennan, Sarah Hamilton and Antony Long
Sea Level Research Unit, Department of Geography, University of Durham, Durham, DH1 3LE, UK
Telephone +44 191 334 1934
Fax +44 191 334 1801
Email ian.shennan@durham.ac.uk
URL http://www.geography.dur.ac.uk

TECHNICAL ABSTRACT

Field and laboratory analyses of tidal marsh sediment sequences at Ocean View, Girdwood and Kenai provide evidence of six great earthquakes in the Greater Anchorage area during the last ~3300 years at intervals ranging from ~400 to ~900 years. Calibration of fossil sequences using diatom transfer functions enable elevation reconstructions of land-level changes associated with each earthquake deformation cycle.

The penultimate great earthquake, ~900 BP, has a different spatial pattern of subsidence compared to AD 1964. It is not recorded at Kenai and subsidence is less at Ocean View, ~0.2 m. Co-seismic subsidence at Girdwood is similar to AD 1964 but pre-seismic subsidence is less. The ~1500 BP great earthquake shows yet another spatial pattern of subsidence. It is of similar magnitude at Girdwood and Ocean View but larger than AD 1964 at Kenai. Different spatial patterns of co-seismic subsidence for the AD 1964, ~900 BP and ~1500 BP great earthquakes may indicate variations in the location or depth of the rupture zone.

Current evidence from older peat-silt contacts indicate subsidence only at Girdwood, during great earthquakes ~2100 BP, ~2500 BP and ~3300 BP.

Observations in AD 1964 recorded no tsunamis at Kenai, Anchorage or Girdwood. There is no litho-stratigraphic or bio-stratigraphic evidence at any of the sites described here to indicate a tsunami within upper Cook Inlet caused by any of the great earthquakes during the last 3300 years.

Diatom analysis of the peat-silt couplets that record six great earthquakes in the last 3300 years provide evidence of pre-seismic land subsidence (relative sea-level rise) for each earthquake. Some of the evidence is more conclusive than others, and we indicate where the signal is possibly enhanced by mixing of sediment and diatoms from the overlying silt into the peat or where the quantitative reconstruction shows a poor modern analogue. Many of the estimates show pre-seismic elevation change smaller than the error term but the fact that it is recorded in the litho- and bio-stratigraphy and the estimates are all negative, indicating relative sea-level rise, rather than a mixture of values either side of zero suggest that this is not a random effect. There is no relationship between the magnitude of pre-seismic and co-seismic subsidence at the same site.

Pre-seismic land subsidence (relative sea-level rise) does appear to be a common feature of late Holocene great earthquakes and seismological models developed on observational data from the last 40 years need to take account of these longer term movements. Quantifiable pre-seismic relative land- and sea-level movements may be a pre-cursor to a great plate-boundary earthquake.

RECURRENT HOLOCENE PALEOSEISMICITY AND ASSOCIATED LAND / SEA LEVEL CHANGES IN THE GREATER ANCHORAGE AREA

Ian Shennan, Sarah Hamilton and Antony Long
Sea Level Research Unit, Department of Geography, University of Durham, DH1 3LE, UK

NON-TECHNICAL ABSTRACT

Field and laboratory analyses of tidal marsh sediment sequences at Ocean View, Girdwood and Kenai provide evidence of six great earthquakes during the last ~3300 years at intervals ranging from ~400 to ~900 years. Different spatial patterns of co-seismic subsidence for the AD 1964, 900 BP and 1500 BP great earthquakes suggest differences in the location or depth of the rupture zone. Diatom analysis provides quantitative evidence of a period of gradual land subsidence (relative sea-level rise) prior to each great earthquake. Quantifiable pre-seismic land subsidence may be a pre-cursor to a great plate-boundary earthquake.

Content

1. Context

1.1 Defining the earthquake deformation cycle in the greater Anchorage area
1.2 Use of microfossils
1.3 Research questions
- **1.3.1** To quantify the vertical resolution of geologic estimates of relative land and sea-level changes from Holocene earthquakes
- **1.3.2** Timing and recurrence interval of Holocene earthquakes around Cook Inlet
- **1.3.3** Evidence for pre-seismic relative sea-level change

2. Field Investigations

3. Methods

3.1 Microfossil analysis
- **3.1.1** Diatom taxonomy note

3.2 Radiocarbon dating
3.3 Numerical techniques

4. Results: Girdwood

4.1 Litho-stratigraphy of Girdwood
4.2 Chrono-stratigraphy of Girdwood
4.3 Bio-stratigraphy of GW-2
4.4 Numerical analysis

5. Results: Ocean View

5.1 Litho-stratigraphy of Ocean View
5.2 Chrono-stratigraphy of Ocean View
5.3 Bio-stratigraphy of peat units at Ocean View
5.5 Numerical analysis

6. Results: Kenai

6.1 Litho- and chrono-stratigraphy of Kenai
6.2 Bio-stratigraphy of Peat A
6.3 Numerical analysis

7. Discussion

7.1 Chronology of great earthquakes
7.2 Pre-seismic relative sea-level rise

Acknowledgements

References

1. Context

Determining the potential for future earthquakes in the U.S. and reducing losses requires knowledge on how often earthquakes have occurred in the past and at what magnitude. This project applies new temporal and vertical techniques to better understand long records of Holocene palaeoseismicity and associated land/sea-level changes in the greater Anchorage area from sedimentary sequences at three sites: Ocean view (Anchorage), Girdwood and Kenai. Evaluating future earthquake risk in the region affected by the great Alaska earthquake of AD 1964 requires knowing how frequently events of this magnitude occur, at what intervals and how the patterns of land movements vary in different events. This project aims to: improve understanding of Holocene ground displacements in the greater Anchorage area; improve the vertical, spatial and temporal resolution of geological estimates of elevation change from Holocene earthquakes in Alaska (with the quantitative methods applicable to Cascadia); determine the recurrence intervals of great earthquakes in the greater Anchorage area; quantify the methods of using microfossil and stratigraphic data in reconstructing Holocene land movements during repeated earthquake cycles; and finally assess the potential of pre-seismic relative sea-level rise as an early warning of an imminent earthquake by identifying its magnitude during multiple Holocene earthquakes at different sites.

Fieldwork in July 2003 collected stratigraphic data from three tidal marshes in, and around the greater Anchorage area: Girdwood, Ocean View (Anchorage) and Kenai (Figure 1.1). We combine the results of this fieldwork with data collected and analysed by Hamilton (2003), Zong *et al*. (2003) and Shennan *et al*. (2003). To address the research questions outlined above and described further in section 1.3 we proposed the following deliverables:

1. Collection of sediment cores or exposed sections to cover two or more late Holocene events at Ocean View (Anchorage), Girdwood and Kenai.
2. Fieldwork at Ocean View (Anchorage), Girdwood and Kenai to assess evidence of any tsunami deposits associated with late Holocene earthquakes within the greater Anchorage area.
3. Microfossil analysis of samples from the three sites.
4. Application of new vertical techniques (quantitative diatom transfer functions) to improve elevation accuracy and resolution of geological estimates of co-seismic and inter-seismic land-level changes from great Holocene earthquakes in Alaska.
5. Analyse evidence for pre-seismic relative sea-level rise.
6. Analyse new radiocarbon dated samples and compare with previously dated material to investigate the coastal extent and recurrence intervals of plate-boundary ruptures.

All of these were achieved and appear in this report.

1.1 Defining the earthquake deformation cycle in the greater Anchorage area

In the greater Anchorage area, the earthquake deformation cycle model (Figure 1.2) could contain up to four main periods (Shennan *et al*., 1999):

1. Rapid co-seismic subsidence (sudden relative sea-level rise) during a large magnitude earthquake
2. Rapid post-seismic uplift (relative sea-level fall) in the following decades
3. Slower inter-seismic uplift (relative sea-level fall) on the timescale of centuries
4. Pre-seismic relative sea-level rise immediately before the next earthquake

Typically, co-seismic subsidence causes freshwater peat to submerge rapidly into the intertidal zone. This results in a peat-silt couplet (Nelson *et al.*, 1996) with peat overlain by fine-grained clastic sediment and a sharp stratigraphic boundary between the two.

Assessment of suddenness and amount of submergence, lateral extent of peat-silt couplets with sharp upper contacts, evidence of tsunami deposits and synchroneity of subsidence with other sites (Nelson *et al*., 1996) are critical in evaluating a possible co-seismic cause.

This work is important if we are to use marsh burial events to determine the frequency and spatial extent of late Holocene co-seismic ground displacements in the greater Anchorage area. Observational data exist relating to the most recent (AD 1964) great plate boundary earthquake in Alaska (Figure 1.1). These data show that co-seismic subsidence varied from <0.5 m to >1.5 m (Plafker, 1969). Girdwood experienced high (>1.5 m) subsidence in AD 1964, whereas Ocean View (Anchorage) lies within the intermediate zone ~0.7 to 1.5 m and Kenai <0.5 m.

1.2 Use of microfossils

Microfossils help distinguish between seismic and non-seismic (e.g. eustasy and glacio-isostasy) origins of peat-silt couplets (e.g. Long and Shennan, 1994; Nelson *et al*., 1996) and the tendency approach (e.g. Shennan, 1986) defines periods within the earthquake deformation cycle model (e.g. Long and Shennan, 1994). A positive sea-level tendency represents an increase in marine influence and a negative sea-level tendency represents a decrease in marine influence. Diatoms are good sea-level indicators as their zonation across the marsh surface relates to tidal inundation and the halobian classification system divides the diatom species into five categories of salt tolerance (Table 1.1).

Table 1.1 The halobian classification scheme of diatoms (Hemphill-Haley, 1993)

Classification	Salinity range (‰)	Description
Polyhalobous (P)	> 30	Marine
Mesohalobous (M)	0.2 to 30	Brackish
Oligohalobous-halophile (O-h)	< 0.2	Freshwater – stimulated at low salinity
Oligohalobous-indifferent (O-i)	< 0.2	Freshwater – tolerates low salinity
Halophobous (H)	0	Salt-intolerant

In broad terms, the order of salinity classes should reflect the change from tidal-flat through salt marsh, to freshwater marsh and bog. The marine (polyhalobous class) and brackish (mesohalobous class) groups usually dominate tidal flat environments and freshwater groups tolerant of different degrees of saline inundation (oligohalobous-halophile and oligohalobous-indifferent classes) become dominant through the transition from salt marsh to freshwater marsh (e.g. Zong *et al*., 2003). Salt-intolerant species (halophobous class) characterise the most landward communities, including acidic bog above the level of the highest tides. No attempt was made to separate out the allochthonous (detrital) and autochthonous (*in situ*) diatoms because we assume that processes acting today are the same as those acting in the past. According to Sawai (2001), the removal of dead diatoms by tidal currents may result in a residual assemblage for the surface tidal flat samples. However, this would also have occurred in the fossil tidal flat samples recorded by the silt units.

We discriminate between the seismic and non-seismic elements of relative sea-level change through the different stages of an earthquake deformation cycle by using a combination of microfossil data collected from modern intertidal and supratidal environments and sediments associated with numerous late Holocene earthquakes from the greater Anchorage area.

1.3 Research questions

The project addresses three research questions:

1.3.1 To quantify the vertical resolution of geologic estimates of relative land and sea-level changes from Holocene earthquakes

Recent investigations in both seismic and non-seismic coastal environments show the potential of quantitative microfossil transfer functions in reconstructing elevation changes (Edwards and Horton, 2000; Horton *et al*., 2000; Gehrels *et al*., 2001). Previous analyses at sites around Cook Inlet (Hamilton, 2003; Zong *et al*., 2003; Shennan *et al.*, 1999; Hamilton and Shennan, in press; Hamilton *et al*., in press; Shennan *et al*., 2003) demonstrate good similarities between many of the fossil assemblages in late Holocene sediments and those collected from transects taken across the modern marshes and tidal flats. Transfer functions lead to quantitative estimates with respect to contemporaneous tide levels for each sediment interval sampled through a complete earthquake deformation cycle and around peat-silt boundaries for multiple earthquakes during the late Holocene.

1.3.2 Timing and recurrence interval of Holocene earthquakes around Cook Inlet

Previous analyses of age and recurrence intervals of late Holocene earthquakes (e.g. Combellick, 1994; Hamilton, 2003) use conventional radiocarbon dating or AMS dating on bulk peat samples. We test the reliability of these dates by comparing bulk peat and *in situ* plant macrofossils from the same samples. There are significant differences (Shennan *et al*., 2003) and so we use AMS dates on *in situ* plant macrofossils to give a revised chronology of great Holocene earthquakes to affect Cook Inlet.

1.3.3 Evidence for pre-seismic relative sea-level change

Microfossil data collected from Alaska and the Cascadia subduction zone (Shennan *et al.,* 1996, 1998; Long and Shennan, 1998; Hamilton, 2003; Shennan *et al*., 2003; Zong *et al*., 2003; Hamilton and Shennan, in press; Hamilton *et al*., in press) indicate relative sea-level rise in the years and decades immediately prior to some late Holocene earthquakes. These observations suggest that pre-seismic relative sea-level rise may be an early warning of an imminent plate boundary earthquake. Identification of inter-seismic and pre-seismic relative sea-level change leading up to the AD 1964 and other late Holocene earthquakes can be applied to current and developing seismic models (e.g. Kato *et al*., 1997; Cohen and Freymueller, 1997; Wyss and Wiemer, 1999; Freymueller *et al*., 2000; Dragert *et al.*, 2001). These models include elements such as seismic quiescence and aseismic slip. They develop from theory but test observations over a limited timescale, typically a few years to a decade. Our evidence will provide an independent test of these models using a much longer timescale, decades to centuries.

2. Field Investigations

Field sampling at Girdwood, Ocean View (Anchorage) and Kenai (Figure 1.1) add to data already collected from previous studies (e.g. Hamilton, 2003; Zong *et al*., 2003; Shennan *et al*., 2003). Combined, these sites cover a 110 km transect in the upper Cook Inlet region and experienced varying amounts of co-seismic displacement in AD 1964, <0.5 to >1.5 m.

We carried out stratigraphic surveys of each marsh using exposed sections and a 25 mm diameter gouge corer. This allowed investigation of marsh litho-stratigraphy using the Troels Smith (1955) scheme of description that characterises the large range of organic and inorganic sediment typical in most coastal lowlands. Levelling of each section and core to local tide level using a standard level and staff and the plotting of marsh stratigraphy allowed the selection and sampling of peat-silt sequences (possibly recording co-seismic subsidence associated with a late Holocene earthquake). Large diameter Russian and piston coring devices and monolith tins were used for sediment sampling and once collected, the sealing

of samples in plastic allowed the transportation of sediment back to Durham for subsequent analyses.

3. Methods

Laboratory work started in October 2003, concentrating on diatom analysis of the fossil sediment samples. The relative land and sea-level changes recorded by the fossil diatoms in the sediment are quantified using the transfer function developed and described in Shennan *et al*. (2003).

3.1 Microfossil analysis

Diatom samples were typically taken at 1 to 2 cm intervals around every peat-silt contact and preparation followed standard laboratory methods (Palmer and Abbott, 1986). A minimum count of 250 diatom valves was possible for most samples. Diatom identification used Van der Werff and Huls (1958-1974) together with supplementary texts of Denys (1991), Hartley *et al*. (1996), Hemphill-Haley (1993) and Patrick and Reimer (1966, 1975). TILIA (version 2.0 b5; Grimm, 1993) allows the plotting of results and the halobian classification system divides the diatom species into five categories of salt tolerance (Table 1.1).

3.1.1 Diatom taxonomy note

We noted differences in the appearance of the genus *Hantzschia* but could not reliably discriminate those that appeared intermediate, in terms of their morphology, between *H. virgata* and *H. amphioxys* as described by Van der Werff and Huls (1958-1974). Therefore, we combine the counts for both forms as *Hantzschia* spp. in both the modern and fossil datasets. *H. virgata* is classified as polyhalobous whereas *H. amphioxys* is oligohalobous (Denys, 1991). Because of these different salinity affinities, combining the counts may potentially decrease the resolution of the transfer function but it is included within the calculated error terms. On the diagrams we show *Hantzschia* spp. as polyhalobous, both in the species plots and in the summary graph. It is important to consider the full diatom assemblage along with the effect of combining these two species, especially where the appearance of *Hantzschia* spp. is the only or main polyhalobous indicator.

3.2 Radiocarbon dating

In situ macrofossils were used for AMS radiocarbon dating. We use further results from Hamilton (2003) provided by the Natural Environment Research Council (NERC) allocation number 935 0901 and our NEHRP External Grant Award #02HQGR0075. CALIB 4.4 (Stuiver and Reimer, 1993) calibrates the radiocarbon results to calendar years before present using the atmospheric decadal data set (file INTCAL98.14C, Stuiver *at al*., 1998) and the 95% probability distribution method. Calibrated ages are referred to in the text and figures as the 95% (2σ) age range.

3.3 Numerical techniques

Numerical techniques establish the relationship between modern diatom data and elevation (m) relative to Mean Higher High Water (MHHW) and allow comparisons between the modern data set and each fossil sample analysed. To accommodate tidal range differences between sites we produce a standardised water level index (SWLI) by standardising elevations relative to Mean Higher High Water and the difference in elevation between Mean Higher High Water and Mean Sea Level (MSL):

$$SWLI_n = \frac{100(h_n - h_{MSL})}{h_{MHHW} - h_{MSL}} + 100$$

Where:
- $SWLI_n$ = standardised water level index for sample n
- h_n = elevation of sample n, m
- h_{MSL} = Mean Sea Level elevation at site, m
- h_{MHHW} = Mean Higher High Water elevation at site, m

We use the transfer function computer program C2 (Juggins, 2003) and modern data from Kenai, Ocean View and Girdwood as described in Shennan *et al*. (2003) and Hamilton and Shennan (in press). For peat layers, the transfer function model uses only modern samples found above a standardised water level index of 225 (Hamilton and Shennan, in press). For silt layers containing *in situ* rootlets, the transfer function model uses only modern samples found above a standardised water level index of 180 and for silt layers containing no rootlets, the transfer function model includes all modern samples. During this study, the transfer function has been updated compared to last year's report to calculate the elevation (m) of the fossil reconstructions to the site specific tidal range rather than that at the closest tide gauge (Hamilton and Shennan, in press). Fossil reconstructions are plotted as each samples elevation (m) relative to MHHW and form the basis for zones shown on diagrams and within tables. Elevation change between two fossil samples is calculated as the difference between the two reconstructed values with an error term defined by (Preuss, 1979):

$\sqrt{(\text{elevation error term } 1^2 + \text{elevation error term } 2^2)}$

The modern analogue technique (MAT) quantifies the similarity between fossil assemblages and the modern training set (Birks *et al*., 1990) and is particularly useful in identifying whether fossil samples possess good modern analogues (e.g. Birks, 1995; Edwards and Horton, 2000; Zong *et al*., 2003). The computer program C2 (Juggins, 2003) models the modern diatom data set against each fossil sample and determines the minimum dissimilarity coefficient for each. Samples with 'poor' modern analogues are highlighted in red in following figures.

The same transfer function was applied to these data to make results directly comparable and in addition, for the AD 1964 earthquake, also applied to data from Shennan *et al.* (1999) and Zong *et al*. (2003).

4. Results: Girdwood

Plafker *et al*. (1969) suggest 1.5 m regional subsidence and up to 0.9 m local subsidence of unconsolidated sediment accompanied the AD 1964 earthquake at Girdwood.

4.1 Litho-stratigraphy of Girdwood

The bank section contains two extensive peat layers, the upper buried in AD 1964 and the lower buried approximately 850 cal yr BP (Shennan *et al*., 2003; Hamilton and Shennan, in press). From two coring transects (GW-1 and GW-2; Figure 4.1) an additional six buried peat-silt couplets are found below present marsh surface (Figure 4.2). This section investigates how the stratigraphy of Girdwood records relative sea- and land-level movements associated with the earthquake deformation cycle. During this project, diatom analysis concentrates on samples from transect GW-2.

4.2 Chrono-stratigraphy of Girdwood

Figure 4.2 and Table 4.1 show radiocarbon (AMS) dates obtained from *in situ* macrofossils found at the top of the buried peat layers at Girdwood. In addition, it shows two conventional ^{14}C dates from tree stumps rooted in the top of peat G, reported by Combellick (1993) close to our site GW-34.

Table 4.1 Radiocarbon results from Girdwood

Lab code	Site	Material	Description	^{14}C age ± 1σ	Calibrated age BP Range of 2σ age probability distribution (and median)	
CAMS-93957	GW-1	Macrofossil	Base of peat H	395±40	318-515	(455)
Beta-45197	GW-34	Rooted wood	Tree stump in peat G	860±60	677-913	(780)
Beta-45199	GW-34	Rooted wood	Tree stump in peat G	940±60	731-954	(848)
CAMS-93958	GW-1	Macrofossil	Top of peat G	955±40	764-948	(856)
Beta-184321	GW-2	Macrofossil	Top of peat G	890±40	714-920	(817)
CAMS-93959	GW-1	Macrofossil	Base of peat G	945±40	744-932	(853)
Beta-184322	GW-2	Macrofossil	Base of peat G	1170±40	971-1175	(1088)
Beta-184326	GW-2	Macrofossil	Top of peat F	1540±40	1334-1523	(1436)
Beta-184323	GW-2	Macrofossil	Base of peat F	2080±40	1934-2148	(2046)
AA-48170	GW-1	Macrofossil	Top of peat E	2140±47	1994-2306	(2125)
Beta-184324	GW-2	Macrofossil	Top of peat E	2120±50	1949-2304	(2094)
CAMS-93960	GW-1	Macrofossil	Base of peat E	2410±35	2346-2709	(2444)
Beta-184325	GW-2	Macrofossil	Base of peat E	2480±50	2360-2727	(2559)
CAMS-93961	GW-1	Macrofossil	Top of peat D	2425±35	2350-2709	(2461)
Beta-184327	GW-2	Macrofossil	Top of peat D	2560±40	2472-2763	(2628)
Beta-184331	GW-2	Macrofossil	Oscillation in peat D	2600±40	2495-2782	(2741)
CAMS-93962	GW-1	Macrofossil	Base of peat D	2500±35	2362-2740	(2575)
Beta-184330	GW-2	Macrofossil	Top of peat C	2530±40	2383-2749	(2588)
Beta-184328	GW-2	Macrofossil	Top of peat B	2710±40	2751-2916	(2812)
Beta-184329	GW-2	Macrofossil	Top of peat A	3040±40	3080-3356	(3251)

4.3 Bio-stratigraphy of GW-2

Tables 4.2 to 4.8 and associated Figures 4.3 to 4.9 describe and illustrate the main changes in diatom assemblages around each individual peat-silt boundary. Depths relate to the sampled sequence, so may be relative to ground level or the top of the core. Elevations relative to a common datum, MHHW, are shown in Figure 4.2.

Peat A

Peat A at GW-2 is a 10 cm thick herbaceous and bryophyte (moss) peat layer with rootlets and stems. A sharp upper boundary separates this peat from the overlying silt. Figure 4.3 illustrates the main diatom changes around the peat-silt boundary and Table 4.2 describes them.

Table 4.2 Diatom assemblages of peat A at GW-2

Zone	Depth (cm)	Diatom description	Lithology
B	366-370.5	Polyhalobous diatoms dominate, e.g. *Cocconeis peltoides*, *Delphineis surirella* and *Paralia sulcata* alongside *Navicula cari* var. *cincta*	Silt
A	370.5-374	Oligohalobous-indifferent and halophobous diatoms dominate, e.g. *Achnanthes minutissima, Cymbella ventricosa* and *Tabellaria flocculosa*. Some polyhalobous species are introduced in the top 2 cm	Peat

Peat B
Peat B at GW-2 is a 17 cm thick herbaceous and bryophyte (moss) peat layer with rootlets, stems and wood. The upper 2 cm contains a small amount of silt and a sharp upper contact separates Peat B from the overlying silt. Diatoms are not preserved below 339.5 cm depth. Figure 4.4 illustrates the changes in bio-stratigraphy and Table 4.3 describes them.

Table 4.3 Diatom assemblages of peat B at GW-2

Zone	Depth (cm)	Diatom description	Lithology
B	334-337.5	Oligohalobous-indifferent species dominate, especially *Fragilaria construens*	Silt
A	337.5-339	Oligohalobous-indifferent species dominate, in particular, *Eunotia pectinalis* and *Fragilaria construens*	Peat

Peat C
Peat C at GW-2 is a 5 cm thick silt-peat with herbaceous rootlets and wood fragments. Figure 4.5 illustrates the changes in bio-stratigraphy and Table 4.4 describes them.

Table 4.4 Diatom assemblages of peat C at GW-2

Zone	Depth (cm)	Diatom description	Lithology
B	324-327.5	Oligohalobous-indifferent species dominate, particularly *Eunotia pectinalis*	Silt
A	327.5-333	No diatoms preserved	Peat

Peat D
Peat D at GW-2 is a 9 cm thick silt-peat unit with a 1 cm silt layer from 305.5 to 304.5 cm. Figure 4.6 illustrates the main changes in diatom assemblages and Table 4.5 describes them. In comparison with the rest of the diatom assemblages, *Hantzschia* spp. in these levels seem likely to be the freshwater form (see section 3.1.1).

Table 4.5 Diatom assemblages of peat D at GW-2

Zone	Depth (cm)	Diatom description	Lithology
B	295-300.5	Polyhalobous diatoms dominate, e.g. *Cocconeis peltoides*, *Delphineis surirella* and *Paralia sulcata*	Silt
A	300.5-307	Oligohalous-indifferent species dominate, e.g. *Cymbella ventricosa*, *Navicula pupula* and *Placoneis elginensis*. Within the top 2 cm, *Gomphonema angustatum* peaks and polyhalobous species increase, e.g. *Delphineis surirella*	Peat

Peat E
Peat E at GW-2 is a 23 cm thick herbaceous and bryophyte (moss) peat unit with rootlets, stems and occasional wood. It has a sharp upper contact with the overlying silt. Figure 4.7

illustrates the diatom assemblages surrounding the peat-silt contact and Table 4.6 describes the main characteristics. No diatoms are preserved below 22 cm.

Table 4.6 Diatom assemblages of peat E at GW-2

Zone	Depth (cm)	Diatom description	Lithology
B	16-21.5	Polyhalobous diatoms dominate at the base, peaking at 19 cm (e.g. *Delphineis surirella* and *Paralia sulcata*). Above this level mesohalobous diatoms increase, especially *Navicula salinarum*	Silt
A	21.5-23	Zone A contains a broad range of diatoms, e.g. *Delphineis surirella*, *Navicula cari* var. *cincta*, *Martyana martyii* and *Tabellaria flocculosa*	Peat

Peat F

Peat F at GW-2 is a 11 cm thick herbaceous and bryophyte (moss) peat unit with rootlets, stems and wood. It has a sharp upper contact with the overlying silt. Figure 4.8 illustrates the main changes in diatom assemblages and Table 4.7 describes them.

Table 4.7 Diatom assemblages of peat F at GW-2

Zone	Depth (cm)	Diatom description	Lithology
B	160-162.5	Polyhalobous diatoms dominate, e.g. *Cocconeis peltoides*, *Delphineis surirella* and *Paralia sulcata* alongside *Navicula cari* var. *cincta*	Silt
A	162.5-166	Oligohalobous-indifferent and halophobous species dominate, e.g. *Achnanthes minutissima* and *Eunotia exigua*	Peat

Peat G

Peat G at GW-2 is a 14 cm thick herbaceous peat layer with a sharp upper contact. Figure 4.9 illustrates the changes in diatom assemblages surrounding the peat-silt contact and Table 4.8 describes them.

Table 4.8 Diatom assemblages of peat G at GW-2

Zone	Depth (cm)	Diatom description	Lithology
B	1-3.5	Polyhalobous diatoms dominate, e.g. *Cocconeis peltoides*, *Delphineis surirella* and *Paralia sulcata*	Silt
A	3.5-7	Halophobous diatoms dominate, e.g. *Eunotia exigua* and *Pinnularia subcapitata*	Peat

4.4 Numerical analysis

This section uses the transfer function and modern analogue technique (MAT) developed and described in Shennan *et al*. (2003) and Hamilton and Shennan (in press). We apply them to the new fossil data collected from GW-2. Figure 4.10 shows the elevation

reconstructions for the fossil samples relative to m MHHW at Girdwood. Samples highlighted in red have poor modern analogues. Diatom assemblages of peat B and C (Figures 4.4 and 4.5) suggest that their burial was not a result of co-seismic subsidence as the diatoms in the overlying silt layer are predominantly freshwater rather than marine. The overlying silt units are also dominated by poor modern analogues and therefore excluded from the summary of earthquakes in Table 4.9. These events are discussed further in section 7.1. Peats A and D contain samples with poor modern analogues but we know that present-day peat-forming environments occur above ~1.15 m MHHW.

Table 4.9 Quantitative estimates of co-seismic subsidence and pre-seismic elevation change along transect Girdwood GW-2

Peat Code	95% Age Range (Cal yr BP)	Co-seismic land elevation change (m)	Pre-seismic land elevation change (m)
G	714-920	-1.59±0.30	-0.02±0.14
F	1334-1523	-1.42±0.29	-0.07±0.13
E	1949-2304	-0.79±0.29	No diatoms preserved
D	2472-2763	-1.48±0.42	-0.43±0.46
C	2383-2749	Non earthquake	Non earthquake
B	2751-2916	Non earthquake	Non earthquake
A	3080-3356	-1.60±0.32	-0.04±0.18

Five definite co-seismic earthquakes are recorded at GW-2 (Table 4.9) over the past ~3300 cal yr BP. Co-seismic subsidence ranges from 0.79±0.29 m (peat E) to 1.60±0.32 m (peat A). Peat D has the largest pre-seismic relative sea-level rise and a distinct diatom assemblage immediately below the peat-silt boundary consisting of *Synedra fasciculata*, *Eunotia lunaris*, *Eunotia pectinalis*, *Gomphonema angustatum*, *Navicula begeri* and *Synedra ulna*. These species either peak or only occur within the top 3 cm of Peat B and so can not be a result of mixing from the overlying silt layer. In contrast, peat A does not have such a distinct diatom assemblage and the relative sea-level rise signal may result in part, or fully, from mixing at the peat-silt boundary. Peats F and G show much smaller changes in oligohalobous species in the top of the peat. Pre-seismic relative sea-level rise could not be quantified for peat E as no diatoms were preserved below the top 1 cm of the peat.

The discussion (Section 7) compares these results from GW-2 with those previously obtained from GW-1 and GW-3 (Hamilton, 2003; Hamilton and Shennan, in press; Shennan *et al*., 2003).

5. Results: Ocean View

From estimates based on mapping in the summers of 1964 and 1965, Plafker (1969) estimates 0.7 to 1.5 m co-seismic subsidence at Anchorage during the AD 1964 earthquake. Before our NEHRP External Grant Award #02HQGR0075 and Hamilton *et al*. (in press) previous work had not identified stratigraphic evidence of the AD 1964 or earlier earthquakes at Ocean View. It is a key location being so close to downtown Anchorage (Figure 1.1).

5.1 Litho-stratigraphy of Ocean View

Coring along three transects at Ocean View (Figure 5.1) reveal up to five buried peat layers with sharp upper contacts and their lateral continuity. A maximum of three buried peat layers are found at Shore Drive and up to five at Coral Lane. Each peat layer is given a name (A at the base, E closest to the surface) to make descriptions of stratigraphy easier. This project concentrates on the deeper peat layers found at Coral Lane with previous analyses concentrating on peats D and E at Shore Drive (Shennan *et al*., 2003; Hamilton *et*

al., in press). The deepest organic units (A and B) comprise banded layers of silt-peat and silt with herbaceous rootlets but it was not possible to correlate separate layers within these units between cores.

5.2 Chrono-stratigraphy of Ocean View

Figure 5.1 and Table 5.1 show radiocarbon (AMS) dates obtained from *in situ* macrofossils found at the top and base of the buried peat layers at Ocean View.

Table 5.1 Radiocarbon results from Ocean View

Lab Code	Site	Material	Stratigraphic context	^{14}C age ± 1σ	Calibrated age BP Range of 2σ age probability distribution (and median)	
Beta-184320	OV-15	macros	Base of peat E	920±40	741-926	(844)
Beta-184310	OV-23	macros	Base of peat D	1510±40	1312-1514	(1393)
Beta-184315	OV-6	macros	Top of peat D	1070±40	929-1056	(980)
Beta-184316	OV-6	macros	Base of peat D	1250±60	1013-1289	(1176)
Beta-184317	OV-2	macros	Top of peat D	940±50	739-946	(850)
Beta-184311	OV-23	macros	Top of peat C	1500±40	1308-1512	(1383)
Beta-184318	OV-2	macros	Top of peat C	1530±40	1333-1520	(1418)
Beta-184319	OV-2	macros	Base of peat C	1720±50	1521-1807	(1627)
Beta-184312	OV-23	macros	Top of unit B	2010±50	1834-2112	(1961)
Beta-184313	OV-23	macros	Middle of unit B	2230±40	2148-2338	(2233)
Beta-184314	OV-23	macros	Top of unit A	2320±40	2158-2458	(2336)

5.3 Bio-stratigraphy of peat units at Ocean View

Tables 5.2 to 5.9 and associated figures (5.2 to 5.9) describe and illustrate the main changes in diatom assemblages around individual peat-silt boundaries.

Unit A

This unit occurs in two cores at the landward end of the Coral Lane transect. At OV-23 it is a 2 cm thick unit consisting of grey organic silt with herbaceous rootlets. It has a sharp upper contact with the overlying silt that contains rare herbaceous rootlets. Figure 5.2 illustrates the main changes in diatom assemblages and Table 5.2 describes them.

Table 5.2 Diatom assemblages of unit A, OV-23

Zone	Depth (cm)	Diatom description	Lithology
A	445-453	No distinct diatom zones occur across lithological changes. A broad range of diatoms dominate throughout, e.g. *Delphineis surirella, Paralia sulcata*, *Navicula cari* var. *cincta, Nitzschia triblionella* and *Nitzschia fruticosa*	Silt and silty peat

Unit B

Unit B consists of silt-peat and silt with varying amounts of herbaceous rootlets. At OV-23 some layers within this unit have sharp upper and sometimes sharp lower contacts. Unit B^1 is the lowest distinguishable organic-rich layer within unit B and consists of a 2 cm thick grey silt with herbaceous rootlets with a sharp upper contact (Figure 5.3 and Table 5.3). Unit B^2

consists of an underlying banded silt unit (386-374 cm), a 10 cm thick (374-364 cm) herbaceous peat with rootlets and silt with a sharp upper contact, a 0.5 cm thick silt unit and an upper herbaceous peat (Figure 5.4 and Table 5.4).

Table 5.3 Diatom assemblages of unit B^1, OV-23

Zone	Depth (cm)	Diatom description	Lithology
B	407-409.5	Polyhalobous and mesohalobous diatoms increase towards the top (e.g. *Delphineis surirella, Paralia sulcata* and *Navicula peregrina*) and oligohalobous-indifferent diatoms decline (e.g. *Diploneis ovalis*, *Navicula tripunctata* and *Rhopalodia gibba*)	Silt
A	409.5-413	There is a general decrease in polyhalobous diatoms towards the top (e.g. *Delphineis surirella* and *Paralia sulcata*) and an increase in oligohalobous-indifferent taxa (e.g. *Epithemia turgida*, *Nitzschia denticula* and *Nitzschia fruticosa*)	Silt and silty peat

Table 5.4 Diatom assemblages of unit B^2, OV-23

Zone	Depth (cm)	Diatom description	Lithology
A	356-386	A broad range of diatoms occur throughout with oligohalobous-indifferent species dominant (e.g. *Eunotia lunaris*, *Navicula pupula* and *Nitzschia fruticosa*). Polyhalobous and mesohalobous species decrease slightly towards the top (e.g. *Delphineis surirella*)	Silt and peat units

Peat C

At OV-2, peat C is a 15 cm thick herbaceous and bryophyte (moss) peat unit whereas at OV-23 it is approximately 70 cm thick and consists of herbaceous peat with *Sphagnum* and rootlets. Figures 5.5 and 5.6 together with tables 5.5 and 5.6 illustrate and describe the main changes in diatom assemblages around the upper peat-silt boundary.

Table 5.5 Diatom assemblages of peat C, OV-2

Zone	Depth (cm)	Diatom description	Lithology
B	272-274.5	Polyhalobous and mesohalobous taxa dominate, e.g. *Delphineis surirella*, *Paralia sulcata* and *Navicula peregrina*	Silt
A	274.5-278	Oligohalobous-indifferent and halophobous diatoms dominate, e.g. *Epithemia turgida, Pinnularia gentilis and Pinnularia subsolaris*. Polyhalobous species increase towards the top, e.g. *Delphineis surirella*	Peat

Table 5.6 Diatom assemblages of peat C, OV-23

Zone	Depth (cm)	Diatom description	Lithology
A	288-295	A broad range of diatoms dominate throughout, e.g. *Delphineis surirella, Paralia sulcata*, *Navicula cari* var. *cincta, Nitzschia triblionella* and *Nitzschia fruticosa.* The diversity of oligohalobous-indifferent and halophobe species declines across the peat-silt contact	Silt and peat

Peat D

Diatom assemblages from peat D at OV-6 are reported in Hamilton *et al*. (in press) and Shennan *et al*. (2003). This study concentrates on diatom assemblages of peat D at OV-15. At OV-15, peat D is a herbaceous peat unit with rootlets and has a sharp upper contact with the overlying silt. Only the top few centimetres were recovered for sampling in this core. Figure 5.7 and Table 5.7 illustrate and describe the main changes in bio-stratigraphy.

Table 5.7 Diatom assemblages of peat D, OV-15

Zone	Depth (cm)	Diatom description	Lithology
B	152-157.5	Polyhalobous and mesohlaobous diatoms dominate, e.g. *Navicula forcipata*, *Navicula peregrina* and *Navicula salinarum*	Silt
A	157.5-159	Oligohalobous-indifferent diatoms dominate, e.g. *Diploneis ovalis*, *Epithemia turgida* and *Navicula tripunctata*	Peat

Peat E

Diatom assemblages from peat E at OV-15a are reported in Hamilton *et al*. (in press) and Shennan *et al*. (2003). This study concentrates on diatom assemblages of peat E at OV-4 and OV-15b. At OV-4 peat E is a 38 cm thick herbaceous peat unit. At OV-15b it is a 84 cm thick herbaceous peat unit with rootlets. Figures 5.8 and 5.9 and Tables 5.8 and 5.9 illustrate and describe changes in diatom assemblages.

Table 5.8 Diatom assemblages of peat E, OV-4

Zone	Depth (cm)	Diatom description	Lithology
B	60-63	*Fragilaria construens* and *Martyana martyi* dominate	Silt
A	63-80	Polyhalobous, mesohalobous and oligohalobous-halophile diatoms decrease towards the top and oligohalobous-indifferent diatoms dominate e.g. *Fragilaria construens* and *Martyana martyi*	Peat

Table 5.9 Diatom assemblages of peat E, OV-15b

Zone	Depth (cm)	Diatom description	Lithology
A	31-43	A broad range of diatoms dominate throughout, e.g. *Paralia sulcata*, *Navicula cari* var. *cincta* and *Nitzschia fruticosa*	Peat and silt

5.4 Numerical Analysis

This section quantifies elevation changes recorded by the bio-stratigraphy of cores taken at Ocean View using the modern training set from Kenai, Ocean View and Girdwood. Figure 5.10 shows the elevation reconstructions for the fossil samples relative to m MHHW at Ocean View using the transfer function. Samples highlighted in red have poor modern analogues and Table 5.10 summarises the results.

Table 5.10 Quantitative estimates of co-seismic subsidence and pre-seismic elevation change at Ocean View

Site	Peat	95% Age Range (Cal yr BP)	Co-seismic land elevation change (m)	Pre-seismic land elevation change (m)
OV-4	E	AD 1964	-0.67±0.43	-0.08±0.23
OV-15b	E	AD 1964	-0.71±0.31	-0.10±0.16
OV-15	D	~900	-0.23±0.32	-0.00±0.19
OV-2	C	1333-1520	-0.99±0.32	-0.07±0.18
OV-23	C	1308-1512	-0.43±0.30	-0.10±0.11
OV-23	B^2	1834-2112	None identified	None identified
OV-23	B^1	2148-2338	None identified	None identified
OV-23	A	2158-2458	None identified	None identified

Units A, B^1 and B^2 do not record any significant elevation change around the lithological boundary. If these units could be traced to other areas of the marsh where the silty peat layers were better developed (more organic, with well-preserved plant macrofossils), they would be a better record to evaluate any co-seismic subsidence but present evidence does not support a co-seismic origin. In contrast, peats C, D and E indicate co-seismic subsidence at the peat-silt boundary due to the large, abrupt change in litho- and bio-stratigraphy and its lateral extent.

Peat C records different amounts of co-seismic subsidence at locations OV-2 and OV-23 (0.99±0.32 m and 0.43±0.30 m respectively). Peat C at OV-2 shows a good pre-seismic signal. Quantitatively, it represents a relative sea-level rise of 0.07±0.18 m and the bio-stratigraphy (Figure 5.5) suggests a distinct diatom assemblage, with peaks in *Cocconeis pediculus*, *Navicula cari* var. *cincta* and *Pinnularia gentilis* within the upper 2 cm of the peat layer. In contrast, OV-23 does not appear have a clear pre-seismic diatom assemblage (Figure 5.6) but the transfer function indicates a pre-seismic elevation change of similar magnitude.

Peat D at OV-15 records 0.23±0.32 m co-seismic subsidence. Quantitative reconstructions suggest no pre-seismic relative sea-level rise but this is inconclusive as the core stopped 3 cm below the peat-silt boundary, hence these changes may not be recorded.

The AD 1964 earthquake (Peat E) at OV-4 and OV-15b record similar amounts of co-seismic subsidence, ~0.69±0.36 m and similar pre-seismic changes, ~0.09±0.19 m. These assume ~2 to 3 cm of mixed sediment and diatom assemblages above the peat-silt contact. The same phenomenon was observed in the previous report at OV-4 and OV-15a (Hamilton *et al*., in press; Shennan *et al*., 2003).

6. Results: Kenai

Plafker (1969) suggests approximately 0.5 m co-seismic subsidence accompanied the AD 1964 earthquake at Kenai but this interpolation was from three observations, at Anchorage, Homer and Nikiski (Figure 1.1). The value for Nikiski, 15 km away, was 0.27 m subsidence.

6.1 Litho-and chrono-stratigraphy of Kenai

A series of cores taken along the modern surface transect at Kenai reveals two to three buried peat layers. Figure 6.1 summarises the litho-stratigraphy across the marsh and radiocarbon dates. Shennan *et al*.(2003) and Hamilton and Shennan (in press) present results from peats A and B. Radiocarbon dates show that the lower peat accumulated ~6500-1575 cal yr BP and the upper peat started to form ~400 cal yr BP (Table 6.1).

Table 6.1 Radiocarbon results from Kenai

Lab Code	Site	Material	Stratigraphic context	^{14}C age ± 1σ	Calibrated age BP Range of 2σ age probability distribution (and median)	
CAMS-93963	KE-7	macros	Base of Peat B	425±40	324-535	(485)
CAMS-93964	KE-7	macros	Top of Peat A	1670±45	1421-1695	(1576)
Beta-184332	KE-5	macros	Top of Peat A	1670±40	1421-1694	(1576)
Beta-184333	KE-5	macros	Base of Peat A	5780±40	6453-6718	(6581)
AA-48152	KE-7	bulk	Base of Peat A	5685±55	6313-6635	(6469)

6.2 Bio-stratigraphy of peat A

Previous analyses investigate the bio-stratigraphy of peat B from locations KE-3, KE-7, KE-8 and KE-13 and peat A from KE-7 (Hamilton, 2003; Zong *et al*., 2003; Hamilton and Shennan, in press; Shennan *et al*., 2003). At KE-7, the upper peat-silt boundary of peat A was transitional over 5 cm, possibly due to erosion and sediment mixing (Hamilton and Shennan, in press; Shennan *et al*., 2003). In all other locations along the coring transect this boundary appears sharp, similar to that observed for the AD 1964 earthquake. This study focuses on the upper peat-silt boundary of peat A at two further locations. Figures 6.2 and 6.3 and Tables 6.2 and 6.3 illustrate and describe diatom assemblages found around the upper peat-silt contact of peat A at KE-5 and KE-15.

Table 6.2 Diatom assemblages of peat A, KE-5

Zone	Depth (cm)	Diatom description	Lithology
B	127-130.5	Contains polyhalobous (e.g. *Cocconeis peltoides*, *Delphineis surirella*, *Paralia sulcata*), mesohalobous (e.g. *Scolioneis tumida*) and oligohalobous-halophile species (e.g. *Navicula cari* var. *cincta). M*esohalobous species (e.g. *Navicula salinarum, Nitzschia filiformis*) increase towards the top	Silt
A	130.5-135	*Eunotia exigua* dominates but declines towards the top with an increase in oligohalobous-indifferent (e.g. *Achnanthes minutissima, Navicula brockmanii, Pinnularia microstauron*) and polyhalobous species (e.g. *Cocconeis peltoides*, *Paralia sulcata*)	Peat

Table 6.3 Diatom assemblages of peat A, KE-15

Zone	Depth (cm)	Diatom description	Lithology
B	151.-154.5	Zone B contains a diverse diatom assemblage including polyhalobous (e.g. *Cocconeis peltoides*, *Delphineis surirella*, *Paralia sulcata*), mesohalobous (e.g. *Navicula peregrina, N. salinarum)* and oligohalobous-halophile species (e.g. *Navicula cari* var. *cincta)*	Silt

A	154.5-159	Halophobous species (e.g. *Tabellaria fenestrata* and *T. flocculosa*) dominate but decline towards the top with an increase in *Fragilariforma constricta*	Peat

6.3 Numerical analysis

This section quantifies elevation changes recorded by the bio-stratigraphy of cores taken at Kenai. Figure 6.4 shows the elevation reconstructions for the fossil samples relative to m MHHW at Kenai. Samples highlighted in red have poor modern analogues and Table 6.4 summaries the results.

Table 6.4 Quantitative estimates of co-seismic subsidence and pre-seismic elevation change at Kenai

Site	Peat	95% Age Range (Cal yr BP)	Co-seismic land elevation change (m)	Pre-seismic land elevation change (m)
KE-5	A	1421-1694	-1.20±0.27	-0.15±0.13
KE-15	A	~1500	-1.11±0.27	-0.05±0.15

Elevation changes around the upper peat-silt contact of peat A at KE-5 and KE-15 are similar (1.20±0.27 m and 1.11±0.27 m respectively). Pre-seismic changes are greater at KE-5 (Table 6.4) as there is a distinct diatom assemblage within the top 1 cm of the peat consisting of a peak in *Achnanthes minutissima*, *Navicula brockmanii* and *Pinnularia microstauron* (Figure 6.2). This assemblage could not be due to mixing from the above silt. At KE-15, the pre-seismic signal is less clear (Figure 6.3) but is still distinct comprising a peak in *Fragilariforma constricta* and a decrease in halophobous taxa. We conclude that these data indicate pre-seismic relative sea-level rise of ~0.1 m, co-seismic subsidence of ~1.2 m and that the transitional changes, previously reported for KE-7, result from sediment reworking and deposition within the palaeo-channel illustrated in the stratigraphic section (Figure 6.1).

7. Discussion

7.1 Chronology of great earthquakes

Comparison of AMS radiocarbon ages on paired samples of bulk peat and *in situ* plant macrofossils show a significant older age for the bulk peat sample in virtually all cases (Figure 7.1). Despite the fact that the ages for the peat layers described in this report may fit with some co-seismic movements reported for Cook Inlet (Combellick, 1994), Copper River Delta and Middleton Island (Plafker *et al*., 1992), it is very clear that no reliable chronology can be based on bulk peat dates (c.f. Bartsch-Winkler and Schmoll, 1992; Combellick, 1994), whether using AMS or conventional radiocarbon methods. A new chronology (Figure 7.2) uses only AMS radiocarbon ages from *in situ* plant macrofossils and two conventional ages on *in situ* tree roots submerged after the penultimate earthquake at Girdwood (Combellick, 1993). We regard these ages as reliable.

There is clear evidence of six great earthquakes during the last ~3300 years at intervals ranging from ~400 to ~900 years (Figure 7.2). Following sections summarise subsidence at Girdwood, Ocean View and Kenai associated with each great earthquake and consider the possibility of further great earthquakes within the record.

Previous analyses suggest that a peat-silt boundary should ideally be sampled and analysed from two or more locations along a section (Hamilton, 2003; Zong *et al*., 2003). This gives a more reliable estimate of co-seismic subsidence as it reduces the possibility of underestimating the magnitude of subsidence if there is a break in sedimentation, erosion at the peat-silt boundary, or the sampling site is towards the local limit of subsidence at the

marsh. Analysis of the AD 1964 earthquake at Kenai (Hamilton, 2003; Zong *et al*., 2003) shows that it is possible to trace the sedimentary expression of subsidence as a silt layer that decreases in thickness in a landward direction. Where this reaches acidic bog or another freshwater swamp environment, beyond the limit of normal post-earthquake high tides, other factors such as local groundwater elevation, pH and nutrient status become as important as elevation with respect to tidal levels. The registration of co-seismic subsidence decreases until it is zero, the point at which the wetland is insensitive to the subsidence.

Table 7.1 Summary of great earthquakes and other subsidence events

Site[1]	Peat code[2]	Age[3]	Co-seismic land elevation change (m)	Pre-seismic land elevation change (m)
GW-1	GW-H	AD 1964	-1.51±0.32	-0.24±0.13
GW33	GW-H	AD 1964	-1.48±0.30	-0.16±0.13
GW34	GW-H	AD 1964	-1.34±0.32	-0.33±0.14
GW99	GW-H	AD 1964	-1.00±0.28	-0.30±0.14
KE-3	KE-B	AD 1964	-0.45±0.28	-0.15±0.13
KE-7	KE-B	AD 1964	-0.73±0.24	-0.11±0.12
KE-8	KE-B	AD 1964	-0.30±0.28	-0.15±0.13
KE-13	KE-B	AD 1964	-0.09±0.13	-0.24±0.13
OV-4	OV-E	AD 1964	-0.67±0.43[b]	-0.08±0.23 [a b]
OV-15b	OV-E	AD 1964	-0.71±0.31	-0.10±0.16 [a]
GW-1	GW-G	900BP	-1.50±0.34	-0.14±0.14
GW-2	GW-G	900BP	-1.59±0.30	-0.02±0.14
OV-15	OV-D	900BP	-0.23±0.32 [b]	too few samples
GW-2	GW-F	1500BP	-1.42±0.29	-0.07±0.13
KE-5	KE-A	1500BP	-1.20±0.27	-0.15±0.13
KE-15	KE-A	1500BP	-1.11±0.27	-0.05±0.15 [b]
KE-7	KE-A	1500BP	sediment mixing	sediment mixing
OV-2	OV-C	1500BP	-0.99±0.32 [b]	-0.07±0.18 [b]
OV-23	OV-C	1500BP	-0.43±0.30	-0.10±0.11 [a b]
OV-23	OV-B[1]	1950BP	None identified	None identified
GW-1	GW-E	2100BP	-1.20±0.34	pollen evidence [c]
GW-2	GW-E	2100BP	-0.79±0.29	too few samples
GW-3	GW-E	2100BP	Non event	Non event
OV-23	OV-B[2]	2200BP	None identified	None identified
OV-23	OV-A	2350BP	None identified	None identified
GW-1	GW-D	2500BP	-1.42±0.34	-0.10±0.18
GW-2	GW-D	2500BP	-1.48±0.42	-0.43±0.46 [b]
GW-2	GW-C	2600BP	Non-seismic	Non-seismic
GW-1	GW-B	2800BP	Non-seismic	Non-seismic
GW-2	GW-B	2800BP	Non-seismic	Non-seismic
GW-1	GW-A	3300BP	-1.36±0.30	-0.01±0.16 [a]
GW-2	GW-A	3300BP	-1.60±0.32	-0.04±0.18 [b]

Notes:
[1] GW-Girdwood, KE-Kenai, OV-Ocean View
[2] Peat layer notations A-H refer to layers at each site but do not indicate chronostratigraphic correlation between Girdwood (GW), Kenai (KE) and Ocean View (OV)
[3] Nominal age, used for ease of reference in following discussions, see previous tables for details of age ranges
[a] no unique diatom assemblage so pre-seismic change may include the effect of mixing from overlying silt.
[b] samples have poor modern analogues. [c] diatoms absent.

To make our estimates more reliable we use results presented in previous sections together with those from our previous investigations (Hamilton, 2003; Shennan *et al.,* 1999; Zong *et al*., 2003; Shennan *et al*., 2003). Table 7.1 summarises elevation changes associated with Holocene great earthquakes and other subsidence events.

For the AD 1964 great earthquake, elevation changes at all three locations derived from our bio-stratigraphic analyses show good agreement with observations taken after the earthquake. They agree with the estimates of 1.5 m, for regional subsidence at Girdwood (Plafker *et al*., 1969), but not any additional subsidence, up to 0.9 m, due to local sediment consolidation recorded for unspecified locations around Girdwood (Plafker *et al*., 1969). All four Girdwood sites record pre-seismic subsidence in the order of ~0.2 m. ^{137}Cs data show that this commenced in the early 1950s (Shennan *et al*., 2003) which coincides with observations of increased tidal flooding of the marshes at Girdwood (Karlstrom, 1964). Estimates for co-seismic subsidence at Ocean View, ~0.7 m, agree with the lower range of measurements around Anchorage 0.7 to 1.5 m (Plafker, 1969) with possible pre-seismic subsidence ~0.1m, but we note the poor modern analogue and the possible effect of sediment mixing (Table 7.1). Reconstructions from Kenai record ~0.3 to 0.7 m co-seismic subsidence for the three sites on the tidal marsh, diminishing to ~0.1 m, from the pre-1964 acidic bog (KE-13). These are similar to the values suggested by Plafker (1969), approximately 0.5 m. All four sites at Kenai show decimetre-scale pre-seismic subsidence.

The penultimate great earthquake, ~900 BP, has a different spatial pattern of subsidence compared to AD 1964 (Figure 7.3). It is not recorded at Kenai and subsidence is less at Ocean View, ~0.2 m. Co-seismic subsidence at Girdwood is similar to AD 1964 but pre-seismic subsidence is less. The ~1500 BP great earthquake shows yet another spatial pattern of subsidence. It is of similar magnitude at Girdwood and Ocean View but larger than AD 1964 at Kenai. Different spatial patterns of co-seismic subsidence for the AD 1964, ~900 BP and ~1500 BP great earthquakes may indicate variations in the location or depth of the rupture zone.

Current evidence from older peat-silt contacts indicate subsidence only at Girdwood, at ~2100 BP, ~2500 BP and ~3300 BP. The section at Kenai (Figure 6.1) records peat accumulation above the limit of tides from ~6500 to 1500 BP with no litho- or bio-stratigraphic evidence of co-seismic subsidence. However, evidence for the ~2100 BP great earthquake at Girdwood (Peat E) suggests that other peat-silt couplets at Girdwood and Ocean View currently shown as non-seismic in origin should be studied further. Sites GW-1, GW-2 and GW-3 lie on the north shore of Turnagain Arm (Figure 4.1). GW-1, closest to the centre of the valley, records the greatest co-seismic subsidence, ~1.2 m, with it diminishing to ~0.8 m at the intermediate site, GW-2. GW-3, closest to the valley side, records an apparently similar lithology, peat with a sharp upper contact overlain by grey silt (Figure 4.2), but the silt records a freshwater diatom assemblage (Hamilton, 2003) for which we have no modern analogue. If the sample from GW-3 were the only one studied for this peat-silt couplet we could not have demonstrated co-seismic subsidence. Current data indicate no support for co-seismic subsidence of Ocean View peat layers OV-A and OV-B. Further transects of cores, radiocarbon dating and diatom analyses will be necessary to test further the hypothesis that they may correlate with the ~2100 BP or ~2500 BP great earthquakes recorded at Girdwood. Similarly, peat layers GW-B and GW-C should be traced across the south side of Glacier Creek to investigate whether they merge to silt with inter-tidal diatom assemblages rather than freshwater assemblages as observed for the ~2100 BP peat, GW-E. This is a critical next step in the investigation since the ages of these peat layers at Ocean View and Girdwood raise the possibility of great earthquakes less than ~100 years apart.

Observations in AD 1964 recorded no tsunamis at Kenai, Anchorage or Girdwood. There is no litho-stratigraphic or bio-stratigraphic evidence at any of the sites described here to

indicate a tsunami within upper Cook Inlet caused by any of the great earthquakes during the last 3300 years.

7.2 Pre-seismic relative sea-level rise

Diatom analysis of the peat-silt couplets that record six great earthquakes in the last 3300 years provide evidence of pre-seismic land subsidence (relative sea-level rise) for each earthquake (Table 7.1). Some of the evidence is more conclusive than others, and we indicate where the signal is possibly enhanced by mixing of sediment and diatoms from the overlying silt into the peat or where the quantitative reconstruction shows a poor modern analogue. Many of the estimates show pre-seismic elevation change smaller than the error term but the fact that it is recorded in the litho- and bio-stratigraphy and the estimates are all negative, indicating land subsidence (relative sea-level rise), rather than a mixture of values either side of zero suggest that this is not a random effect. If pre-seismic land subsidence (relative sea-level rise) is a precursor to a great earthquake, it seems that there is no relationship between the magnitude of pre-seismic and co-seismic subsidence at the same site (Figure 7.4).

In addition, Karlstrom (1964) observed that at Girdwood, storm tides that did not flood the marsh surface before AD 1953 began depositing a thin surface layer of silt that became progressively thicker each year. This date corresponds to the start of the pre-seismic signal identified from the microfossil data at Girdwood, dated using ^{137}Cs. There was no tide gauge at Anchorage before the AD 1964 great earthquake but there were at Women's Bay (Kodiak Island) and Seward (Kenai Peninsula). Both locations experienced co-seismic subsidence associated with the AD 1964 great earthquake but the tide gauge measurements did not register any quantifiable pre-seismic relative sea-level rise (Savage and Plafker, 1991). One explanation for the conflicting evidence of pre-seismic change, is that there was differential movement between sites in the same way that post-seismic recovery is spatially variable. For example, GPS measurements indicate a different direction and rate of present day movement between Seward and Anchorage against sites along the western Kenai Peninsula (Cohen and Freymueller, 2001).

Other possible explanations for apparent pre-seismic relative sea-level rise include a temporary change in sea level due to the El Nino Southern Oscillation (ENSO). ENSO can cause higher water levels along the west coast of the USA and Alaska, for example, the AD 1997-1998 El Nino caused a short-lived sea-level rise during the winter of approximately 0.20 m at Seldovia and Seward, Alaska (data from http://www.pmel.noaa.gov). Any effect before the AD 1964 great earthquake would be as short lived and the magnitude would be even smaller as the only El Nino as large as AD 1997-1998 occurred in AD 1940-1942. Observations at Girdwood by Karlstrom (1964) suggest that the relative sea-level rise started in AD 1953 corresponds to an El Nino peak but it could not account for continued flooding of the marsh surface he observed between AD1954 and 1957 when El Nino was weak. The short-term effect could not account for a relative sea-level rise over the period of several years to a decade and it is hard to envisage how such a process could occur before every peat-silt boundary.

If it does form part of the earthquake deformation cycle model and occurs over several years to a decade, possible mechanisms of pre-seismic land subsidence (relative sea-level rise) include aseismic slip (e.g. Dragert *et al*., 2001; Miller *et al*., 2002). Furthermore, tide gauge data in Japan (Katsumata *et al*., 2002) record several centimetres of aseismic subsidence during a five year period before the AD 1994 Hokkaido-Toho-Oki earthquake (magnitude 8.3). Other possible mechanisms include certain seismic quiescence models (e.g. Kato *et al*., 1997; Wyss *et al*., 1981; Dieterich and Okubu, 1996). Pre-seismic land subsidence (relative sea-level rise) does appear to be a common feature of late Holocene great earthquakes; seismological models developed on observational data need to take account of

these longer term movements. Quantifiable pre-seismic land subsidence (relative sea-level rise) may be a pre-cursor to a great plate-boundary earthquake.

Acknowledgements
This research was also partially supported by: the U.S. Geological Survey, Department of the Interior; NERC Research Studentship GT 04/99/ES/57; NERC radiocarbon allocation number 935 0901. We also wish to acknowledge help from the technicians from the Geography Department, University of Durham; Design and Imaging Unit, University of Durham; Sir James Knott Foundation Fellowship; and Smiley Shields, Anchorage.

References

Bartsch-Winkler, S. & Schmoll, H. R., 1992. Utility of radiocarbon dated stratigraphy in determining late Holocene earthquake recurrence intervals, upper Cook Inlet region, Alaska. *Geological Society of America Bulletin*, **104**, 684-694.

Birks, H. J. B., 1995. Quantitative palaeoenvironmental reconstructions. In: *Statistical modelling of Quaternary science data.* (eds Maddy, D. & Brew, J. S.) *Technical Guide No.5*, pp. 161-254, Quaternary Research Association, London.

Birks, H. J. B., Line, J. M., Juggins, S., Stevenson, A. C. & ter Braak, C. J. F., 1990. Diatoms and pH reconstruction. *Philosophical Transactions of the Royal Society of London B*, **327**, 263-278.

Cohen, S. C. & Freymueller, J. T., 1997. Deformation of the Kenai Peninsula, Alaska. *Journal of Geophysical Research*, **102**, 20,479-420,487.

Cohen, S. C. & Freymueller, J. T., 2001. Crustal uplift in the south central Alaska subduction zone: new analysis and interpretation of tide gauge observations. *Journal of Geophysical Research*, **106**, 11,259-211,270.

Combellick, R. A., 1994. Investigation of peat stratigraphy in tidal marshes along Cook Inlet, Alaska, to determine the frequency of 1964-style great earthquakes in the Anchorage region. *Alaska Division of Geological and Geophysical Surveys Report of Investigations*, **94-7**, 1-24.

Combellick, R. A. & Reger, R. D., 1994. Sedimentological and radiocarbon age data for tidal marshes along eastern and upper Cook Inlet, Alaska. *Alaska Division of Geological and Geophysical Surveys Report of Investigations*, **94-6**, 1-60.

Denys, L., 1991. A checklist of the diatoms in the Holocene deposits of the western Belgian coastal plain with a survey of their apparent ecological requirements. *Belgian Geological Survey Professional Paper 1991/2*, **246**, 1-41.

Dieterich, J. H. & Okubu, P. G., 1996. An unusual pattern of recurring seismic quiescence at Kalapana, Hawaii. *Geophysical Research Letters*, **23**, 447-450.

Dragert, H., Wang, K. & James, T. S., 2001. A silent slip event on the deeper Cascadia subduction interface. *Science*, **292**, 1525-1528.

Edwards, R. J. & Horton, B. P., 2000. Reconstructing relative sea-level change using UK salt-marsh foraminifera. *Marine Geology*, **169**, 41-56.

Freymueller, J. T., Cohen, S. & Fletcher, H. J., 2000. Spatial variations in present-day deformation, Kenai Peninsula, Alaska, and their implications. *Journal of Geophysical Research*, **105**, 8079-8101.

Gehrels, W. R., Roe, H. M. & Charman, D. J., 2001. Foraminifera, testate amoebae and diatoms as sea-level indicators in UK salt marshes: a quantitative multiproxy approach. *Journal of Quaternary Science*, **16**, 201-220.

Grimm, E., 1993. *TILIA: A pollen program for analysis and display*. Illinois State Museum, Springfield

Hamilton, S. L., 2003. *Late Holocene relative sea-level changes and earthquakes around the upper Cook Inlet, Alaska, USA.* Unpublished PhD Thesis, University of Durham, Durham, UK.

Hamilton, S.L. & Shennan, I. (in press 2005). Late Holocene land and sea-level changes and the earthquake deformation cycle around upper Cook Inlet, Alaska. *Quaternary Science Reviews*.

Hamilton, S.L., Shennan, I., Combellick, R., Mulholland, J. & Noble, C. (in press 2005). Evidence of two great earthquakes at Anchorage, Alaska and implications for multiple events through the Holocene. *Quaternary Science Reviews*.

Hartley, B., Barber, H. G. & Carter, J. R., 1996. *An atlas of British diatoms*. Biopress, Bristol, 601pp.

Hemphill-Haley, E., 1993. Taxonomy of recent and fossil (Holocene) diatoms (Bacillariophyta) from northern Willapa Bay, Washington. *US Geological Survey Open File Report*, **93-289**, 1-151.

Horton, B. P., Edwards, R. J. & Lloyd, J. M., 2000. Implications of a microfossil based transfer function in Holocene sea-level studies. In: *Holocene land-ocean interaction and environmental change around the North Sea.* (eds Shennan, I. & Andrews, J.), pp. 41-54, Geological Society, London.

Juggins, S., 2003. *C^2 User guide*. *Software for ecological and palaeoecological data analysis and visualisation.* University of Newcastle, Newcastle upon Tyne, UK. 69pp.

Karlstrom, T. N. V., 1964. Quaternary geology of the Kenai lowland and the glacial history of Cook Inlet region, Alaska. *US Geological Survey Professional Paper*, **443**, 1-69.

Kato, N., Ohtake, M. & Hirasawa, T., 1997. Possible mechanisms of precursory seismic quiescence: Regional stress relaxation due to preseismic sliding. *Pure and Applied Geophysics*, **150**, 249-267.

Katsumata, K., Kasahara, M., Ozawa, S. & Ivashchenko, A., 2002. A five years super-slow aseismic precursor model for the 1994 M8.3 Hokkaido-Toho-Oki lithospheric earthquake based on tide gauge data. *Geophysical Research Letters*, **29**, 32-1 – 32-4.

Long, A. J. & Shennan, I., 1994. Sea-level changes in Washington and Oregon and the "Earthquake deformation cycle". *Journal of Coastal Research*, **10**, 825-838.

Long, A. J. & Shennan, I., 1998. Models of rapid relative sea-level change in Washington and Oregon, USA. *The Holocene*, **8**, 129-142.

Miller, M. M., Melbourne, T., Johnson, D. J. & Sumner, W. Q., 2002. Periodic slow earthquakes from the Cascadia subduction zone. *Science*, **295**, 2423.

Nelson, A. R., Shennan, I. & Long, A. J., 1996. Identifying coseismic subsidence in tidal-wetland stratigraphic sequences at the Cascadia subduction zone of western North America. *Journal of Geophysical Research*, **101**, 6115-6135.

Palmer, A. J. & Abbott, W. H., 1986. Diatoms as indicators of sea-level change. In: *Sea Level Research: a manual for the collection and evaluation of data* (ed Van de Plassche, O.), pp. 457-488, Geobooks, Norwich.

Patrick, R. & Reimer, C. W., 1966. *The Diatoms of the United States. Volume 1. Monographs of The Academy of Natural Sciences of Philadelphia No 13*. Academy of Natural Sciences of Philadelphia, Philadelphia, 688pp.

Patrick, R. & Reimer, C. W., 1975. *The Diatoms of the United States. Volume 2, Part 1. Monographs of The Academy of Natural Sciences of Philadelphia No 13*. The Academy of Natural Sciences of Philadelphia, Philadelphia, 213pp.

Plafker, G., 1969. Tectonics of the March 27, 1964, Alaska earthquake. *US Geological Survey Professional Paper*, **543-1**, 1-74.

Plafker, G., Kachadoorian, R., Eckel, E. B. & Mayo, L. R., 1969. Effects of the earthquake of March 27, 1964 on various communities. *US Geological Survey Professional Paper*, **542-G**, 1-50.

Plafker, G., Lajoie, K. R. & Rubin, M., 1992. Determining intervals of great subduction zone earthquakes in southern Alaska by radiocarbon dating. In: *Radiocarbon after four decades. An interdisciplinary perspective* (eds Taylor, R. E., Long, A. & Kra, R. S.), pp. 436-452, Springer Verlag, New York.

Preuss, H., 1979. Progress in computer evaluation of sea-level data within the IGCP project no. 61. In: *International Symposium on coastal evolution in the Quaternary, September 11-18, 1978* (eds Suguio, K., Fairchild, T. R., Martin, L. & Flexor, J.), pp. 104-134, Sao-Paulo, Brazil.

Savage, J. C. & Plafker, G., 1991. Tide gage measurements of uplift along the south coast of Alaska. *Journal of Geophysical Research*, **96**, 4325-4336.

Sawai, Y., 2001. Distribution of living and dead diatoms in tidal wetlands of northern Japan: relations to taphonomy. *Palaeogeography, Palaeoclimatology, Palaeoecology*, **173**, 125-141.

Shennan, I., 1986. Flandrian sea-level changes in the Fenland II. Tendencies of sea-level movement, altitudinal changes and local and regional factors. *Journal of Quaternary Science*, **1**, 155-179.

Shennan, I., Long, A. J., Rutherford, M. M., Green, F. M., Innes, J. B., Lloyd, J. M., Zong, Y. & Walker, K., 1996. Tidal marsh stratigraphy, sea-level change and large earthquakes, I: a 5000 year record in Washington USA. *Quaternary Science Reviews*, **15**, 1023-1059.

Shennan, I., Long, A. J., Rutherford, M. M., Kirkby, J., Green, F. M., Innes, J. B. & Walker, K., 1998. Tidal marsh stratigraphy, sea-level change and large earthquakes, II: events during the last 3500 years at Netarts Bay, Oregon, USA. *Quaternary Science Reviews*, **17**, 365-393.

Shennan, I., Scott, D., Rutherford, M. & Zong, Y., 1999. Microfossil analysis of sediments representing the 1964 earthquake, exposed at Girdwood Flats, Alaska, USA. *Quaternary International*, **60**, 55-73.

Shennan, I., Hamilton, S.L. & Long, A.J., 2003. Late Holocene Paleoseismicity and associated land / sea level change in the greater Anchorage area. USGS NEHRP External Grant Award # 02HQGR0075 Final Report.

Stuiver, M. & Reimer, P. J., 1993. Extended 14C database and revised CALIB 3.0 radiocarbon calibration program. *Radiocarbon*, **35**, 215-230.

Stuiver, M., Reimer, P. J., Bard, E., Beck, J. W., Burr, G. S., Hughen, K. A., Kromer, B., McCormac, F. G., v.d.Plicht, J. & Spurk, M., 1998. INTCAL98 Radiocarbon age calibration 24,000 - 0 cal BP. *Radiocarbon*, **40**, 1041-1083.

Troels-Smith, J., 1955. Characterisation on unconsolidated sediments. *Danmarks Geologiske Undersogelse*, **IV**, series 3, 1-73.

Van der Werff, A. & Huls, H., 1958-1974. *Diatomeeenflora van Nederland. 8 parts.* Published privately, De Hoef, The Netherlands.,

Wyss, M., Klein, F. W. & Johnston, A. C., 1981. Precursors to the Kalapana M=7.2 earthquake. *Journal of Geophysical Research*, **86**, 3881-3900.

Wyss, M. & Wiemer, S., 1999. How can one test the seismic gap hypothesis? The case of repeated ruptures in the Aleutians. *Pure and Applied Geophysics*, **155**, 259-278.

Zong, Y., Shennan, I., Combellick, R. A., Hamilton, S.L. & Rutherford, M.M., 2003. Microfossil evidence for land movements associated with the AD 1964 Alaska earthquake. *The Holocene*, **13**, 7-20.

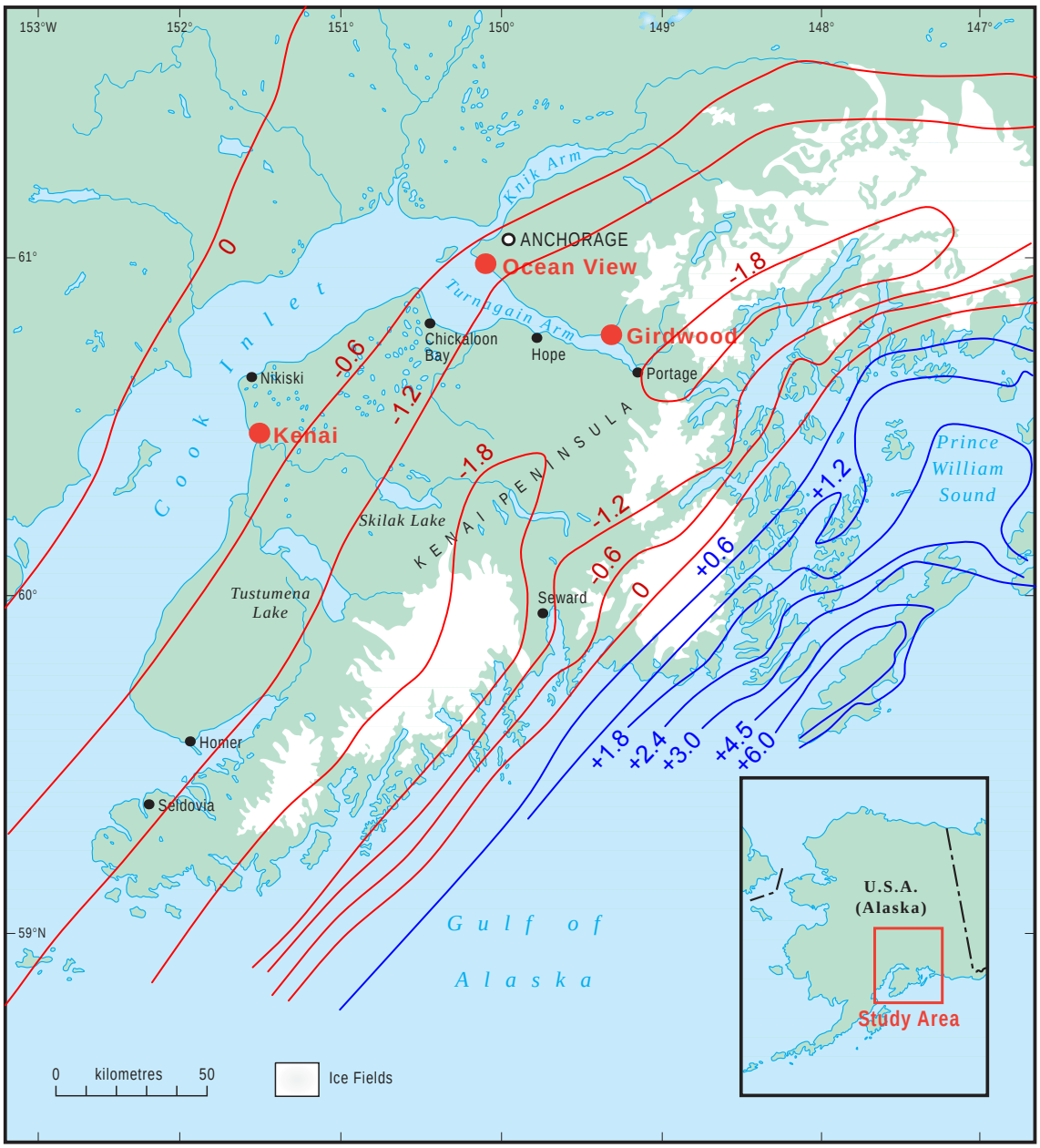

Figure 1.1
Location of field sites around Cook Inlet. Contours (m) show vertical deformation caused by the AD 1964 earthquake, modified from Plafker (1969). The contours hide many local scale variations, including local subsidence caused by sediment compaction and, in addition, some are based on interpolations over long distances.

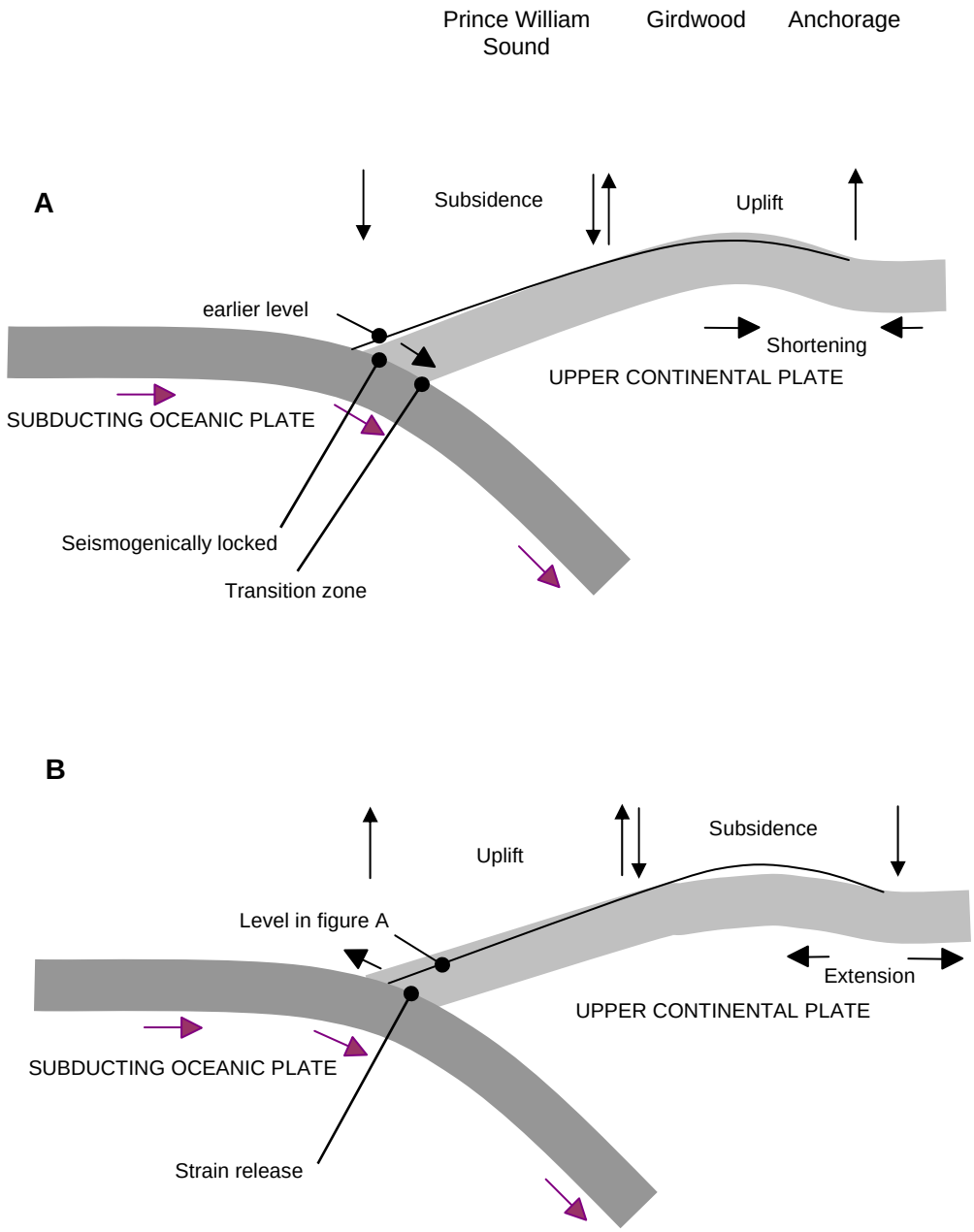

Figure 1.2

Schematic diagrams showing the pattern of (A) inter-seismic and (B) co-seismic deformation associated with a subduction zone earthquake. Adapted from Nelson *et al*. (1996) to reflect the spatial pattern of co-seismic deformation during the AD 1964 earthquake in Alaska. Site locations are in Figure 1.1.

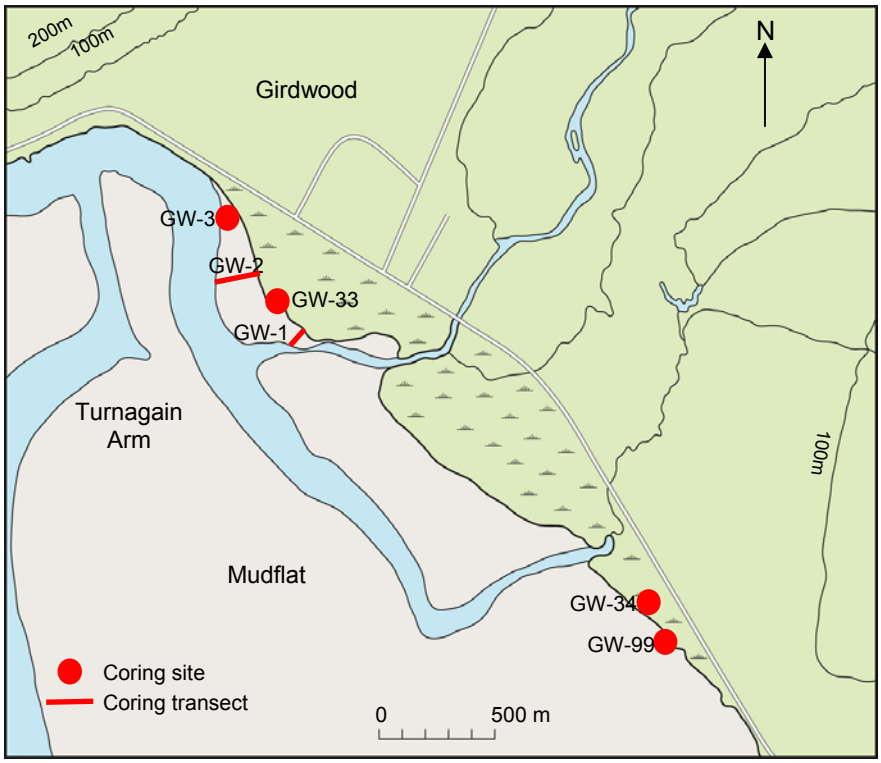

Figure 4.1
Location of sampling sites GW-1 and GW-2 at Girdwood. GW-33 and 34 are sites reported by Zong *et al*. (2003) and GW-99 by Shennan *et al*. (1999).

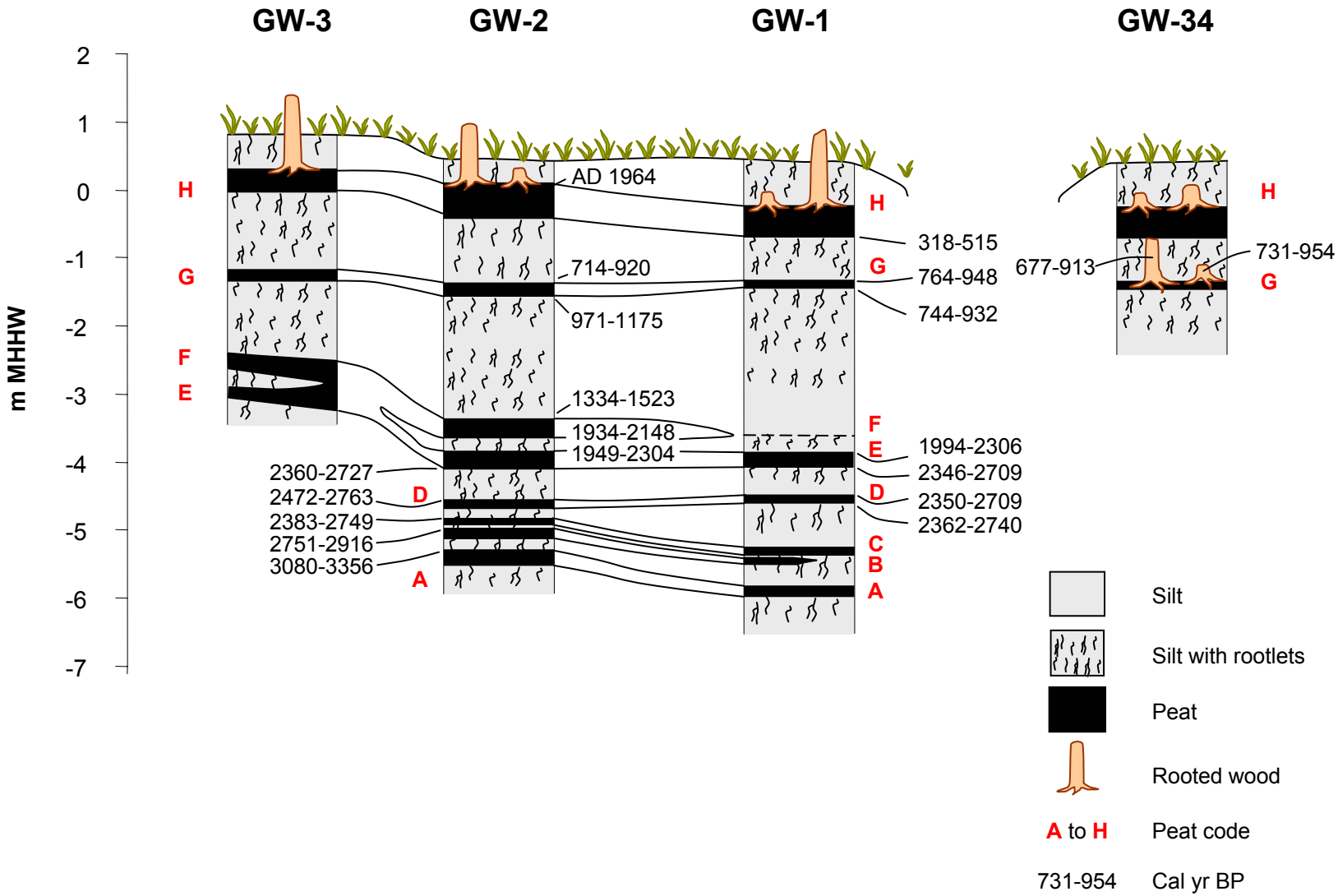

Figure 4.2
Composite section showing the buried peat layers beneath the marsh surface at Girdwood.

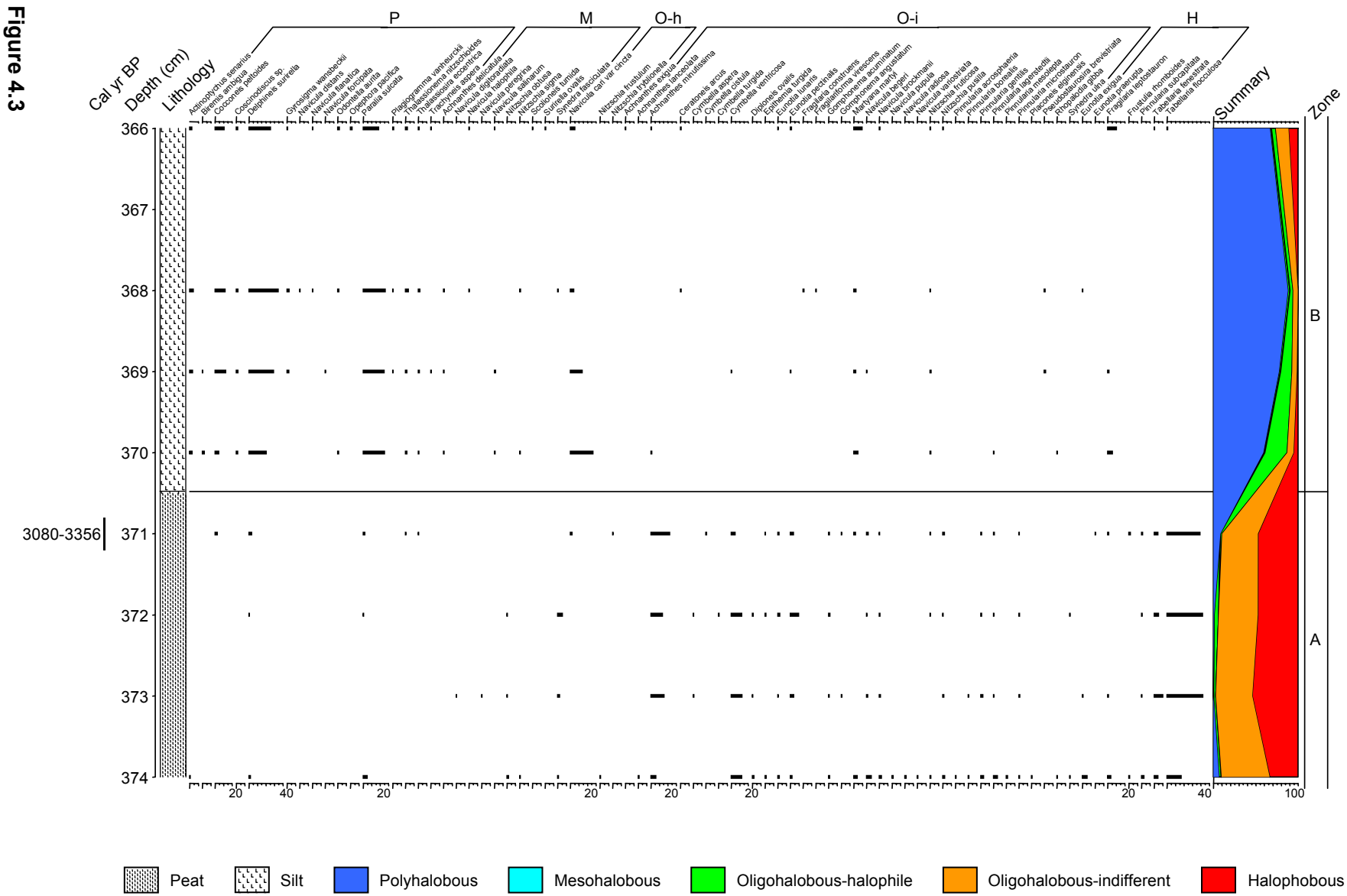

Figure 4.3
Bio-stratigraphy of peat A, GW-2 showing all diatoms counted. P: polyhalobous, M: mesohalobous, O-h: oligohalobous-halophile, O-i: oligohalobous-indifferent, H: halophobous diatom salinity groups ordered left to right in summary graph.

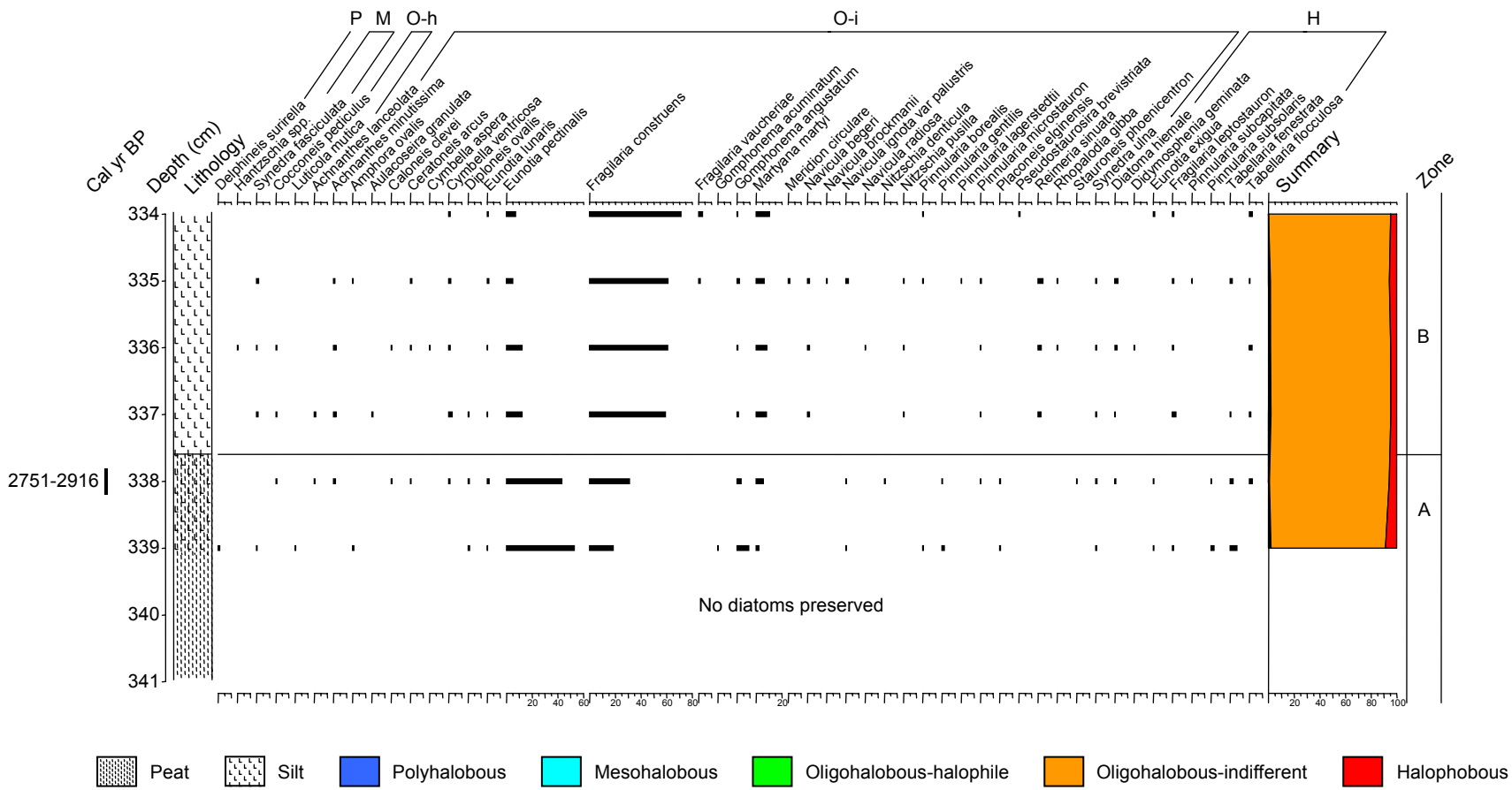

Figure 4.4
Bio-stratigraphy of peat B, GW-2 showing all diatoms counted. P: polyhalobous, M: mesohalobous, O-h: oligohalobous-halophile, O-i: oligohalobous-indifferent, H: halophobous diatom salinity groups ordered left to right in summary graph.

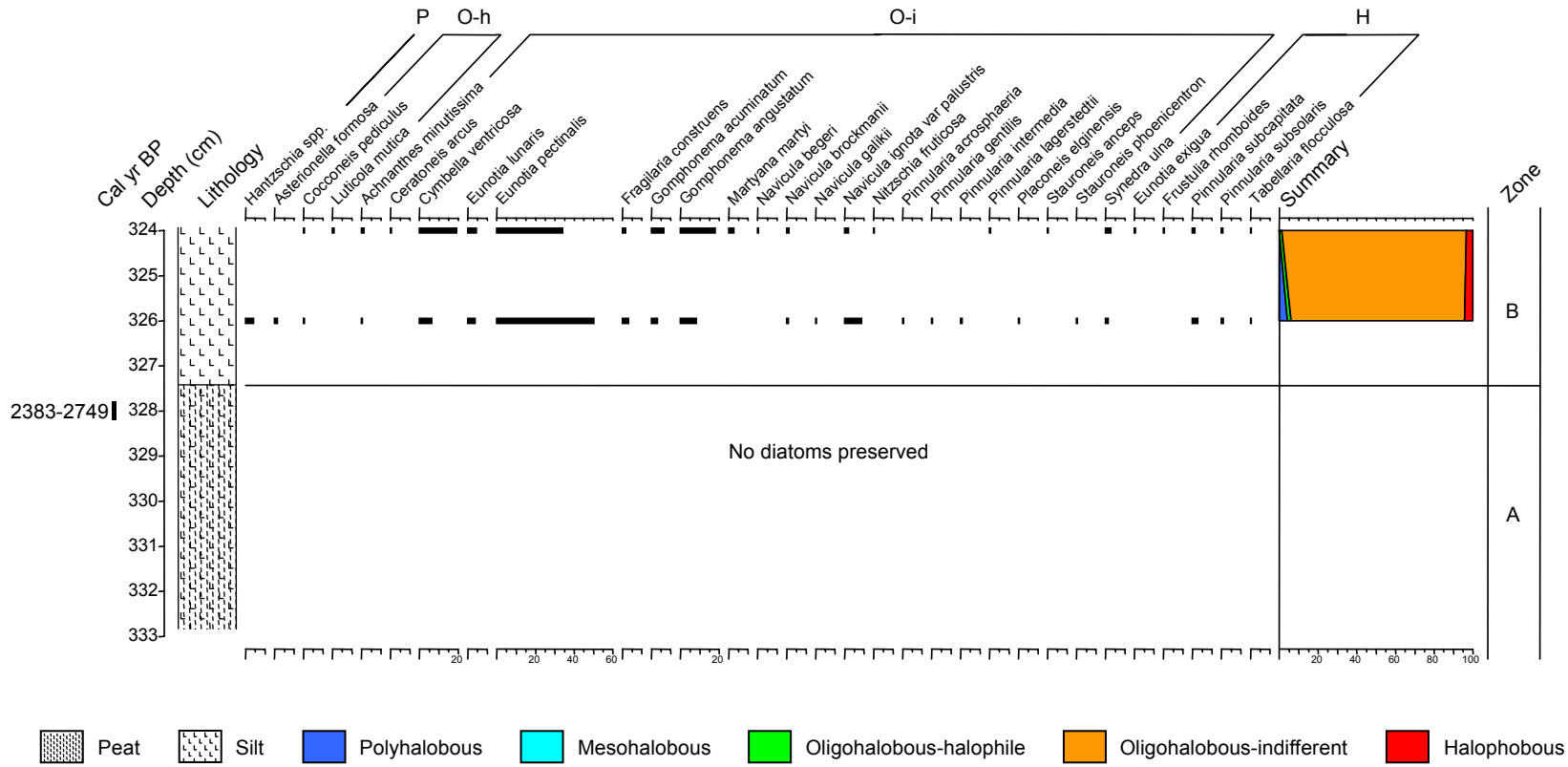

Figure 4.5
Bio-stratigraphy of peat C, GW-2 showing all diatoms counted. P: polyhalobous, M: mesohalobous, O-h: oligohalobous-halophile, O-i: oligohalobous-indifferent, H: halophobous diatom salinity groups ordered left to right in summary graph.

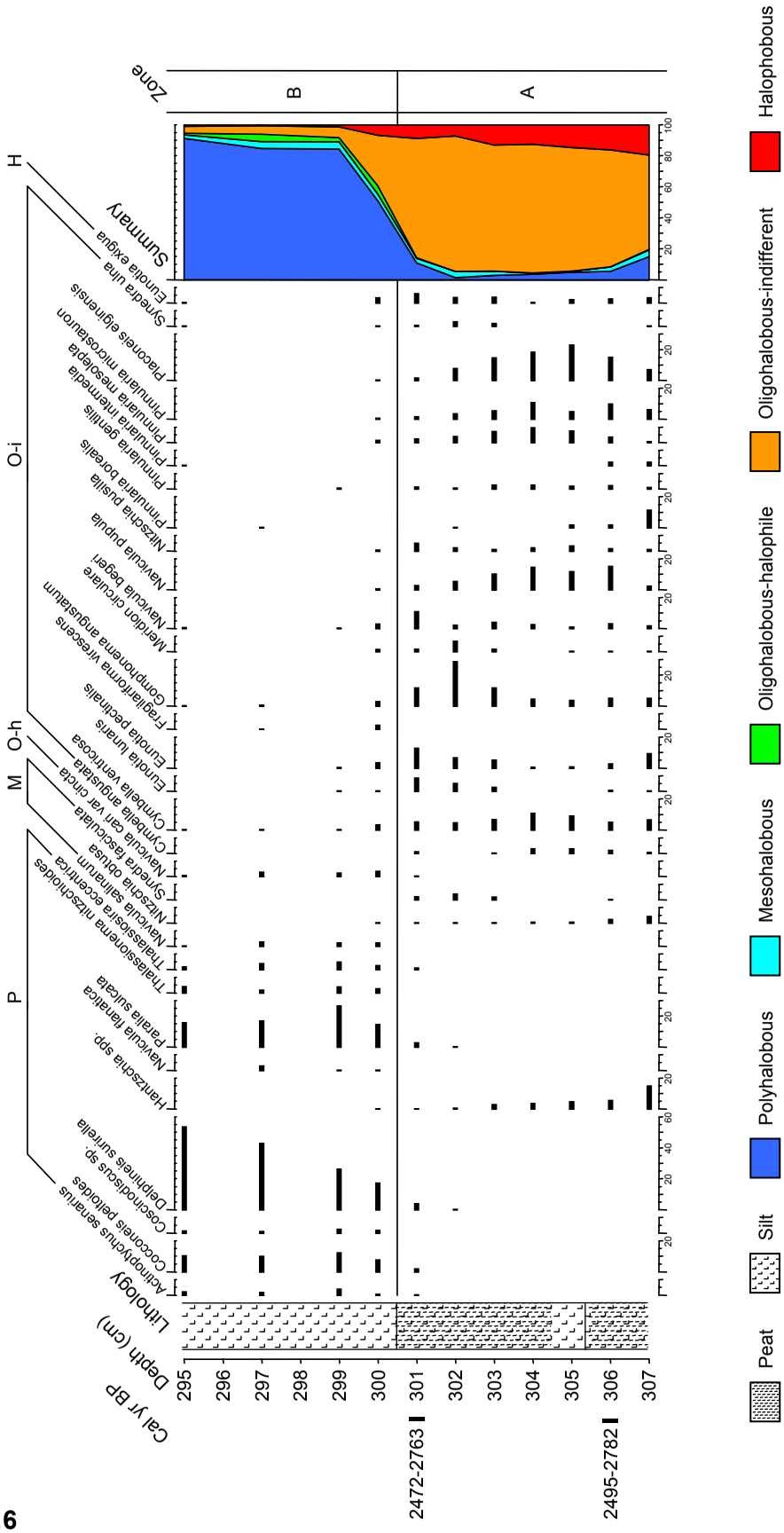

Figure 4.6

Bio-stratigraphy of peat D, GW-2 showing 2% total diatom valves counted. P: polyhalobous, M: mesohalobous, O-h: oligohalobous-halophile, O-i: oligohalobous-indifferent, H: halophobous diatom salinity groups ordered left to right in summary graph.

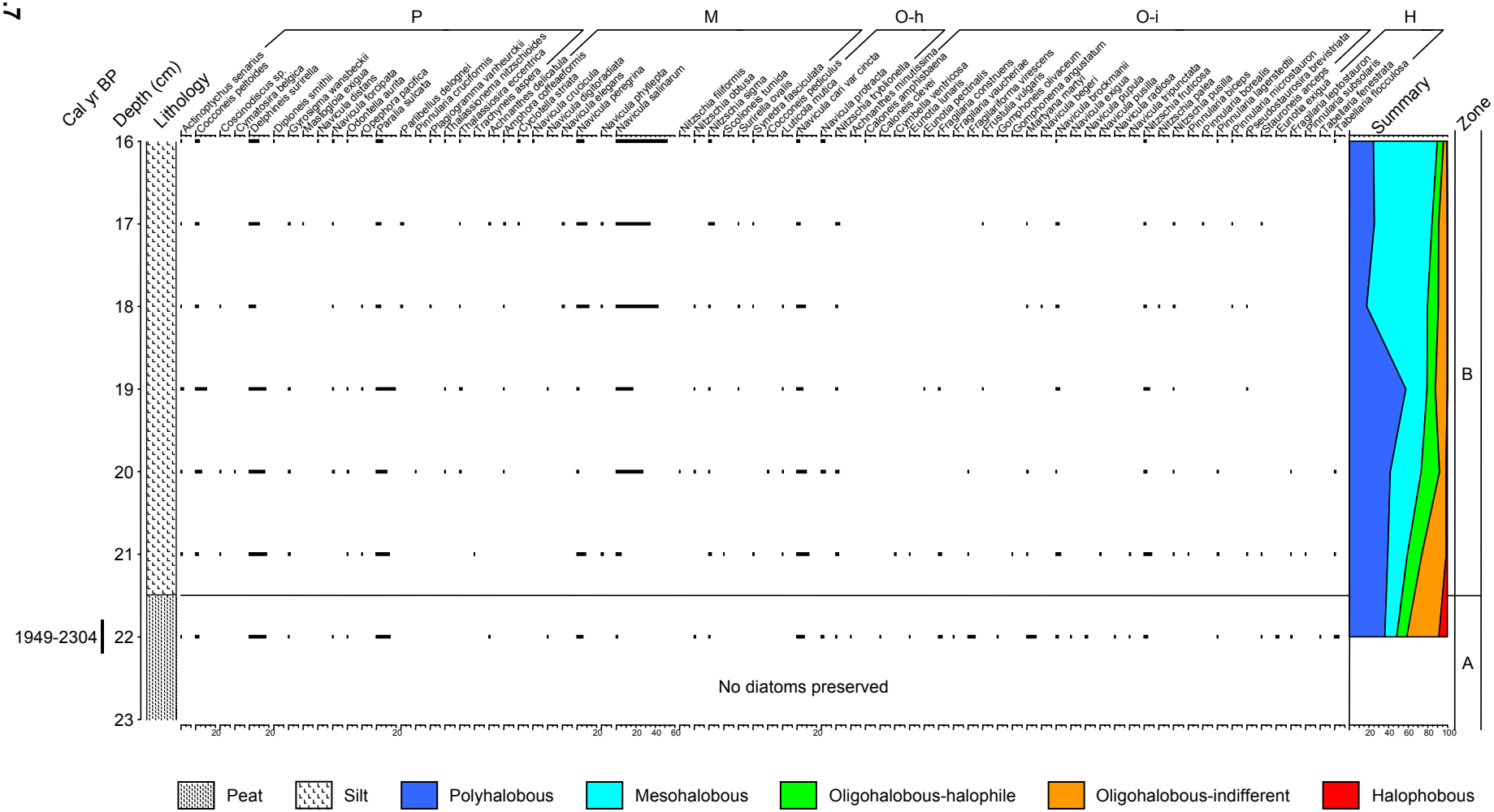

Figure 4.7
Bio-stratigraphy of peat E, GW-2 showing all diatoms counted. P: polyhalobous, M: mesohalobous, O-h: oligohalobous-halophile, O-i: oligohalobous-indifferent, H: halophobous diatom salinity groups ordered left to right in summary graph.

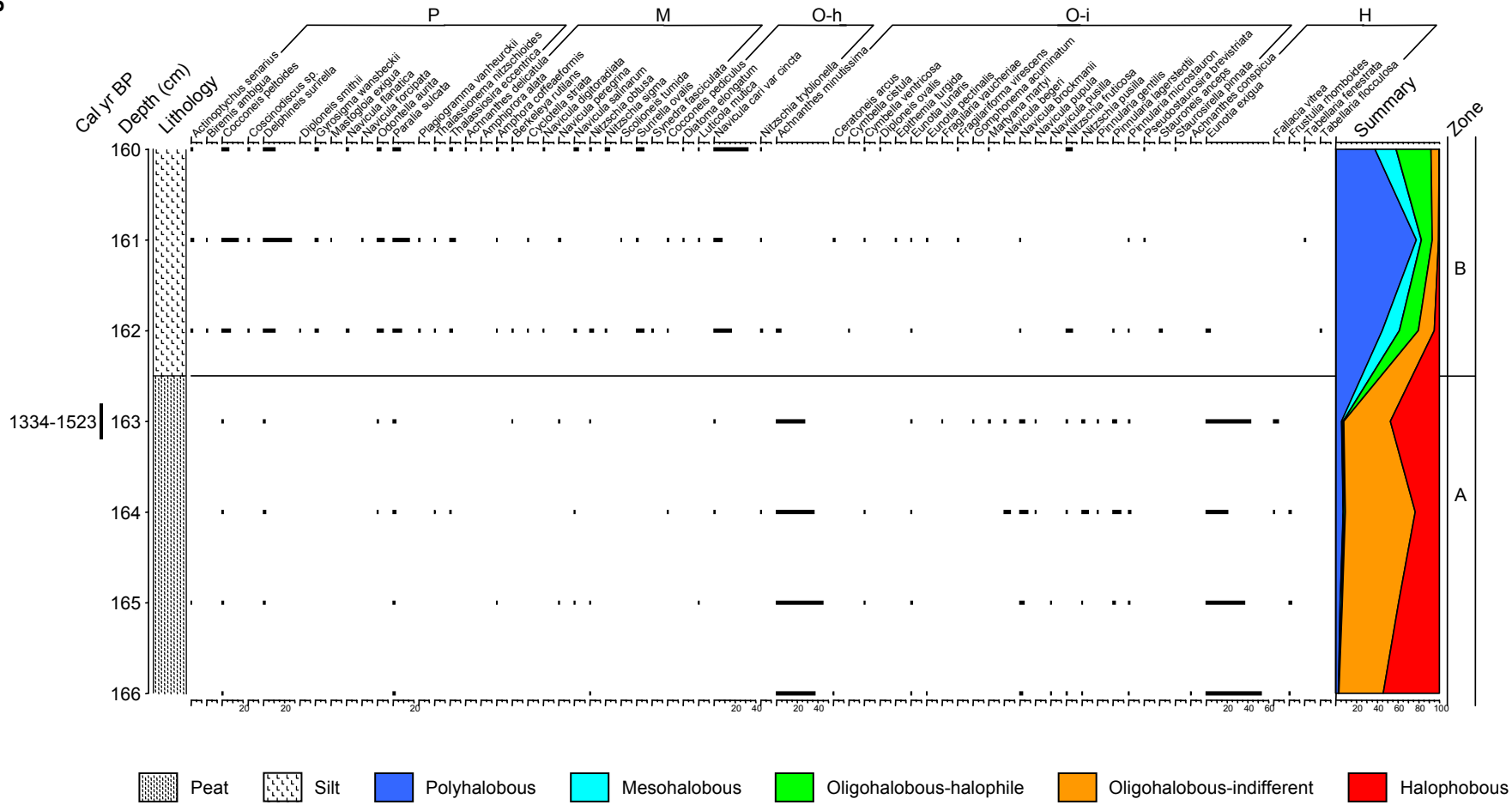

Figure 4.8

Bio-stratigraphy of peat F, GW-2 showing all diatoms counted. P: polyhalobous, M: mesohalobous, O-h: oligohalobous-halophile, O-i: oligohalobous-indifferent, H: halophobous diatom salinity groups ordered left to right in summary graph.

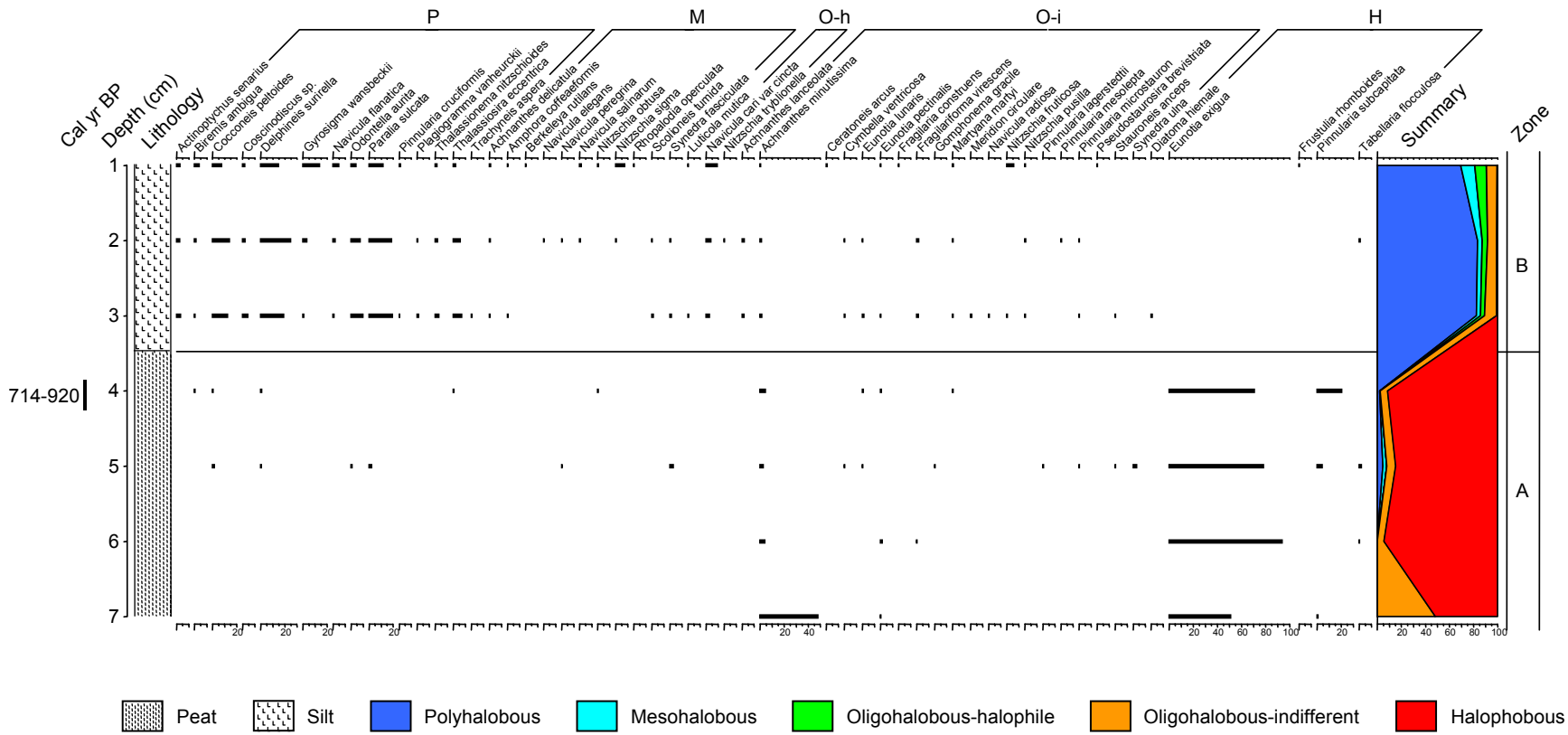

Figure 4.9
Bio-stratigraphy of peat G, GW-2 showing all diatoms counted. P: polyhalobous, M: mesohalobous, O-h: oligohalobous-halophile, O-i: oligohalobous-indifferent, H: halophobous diatom salinity groups ordered left to right in summary graph.

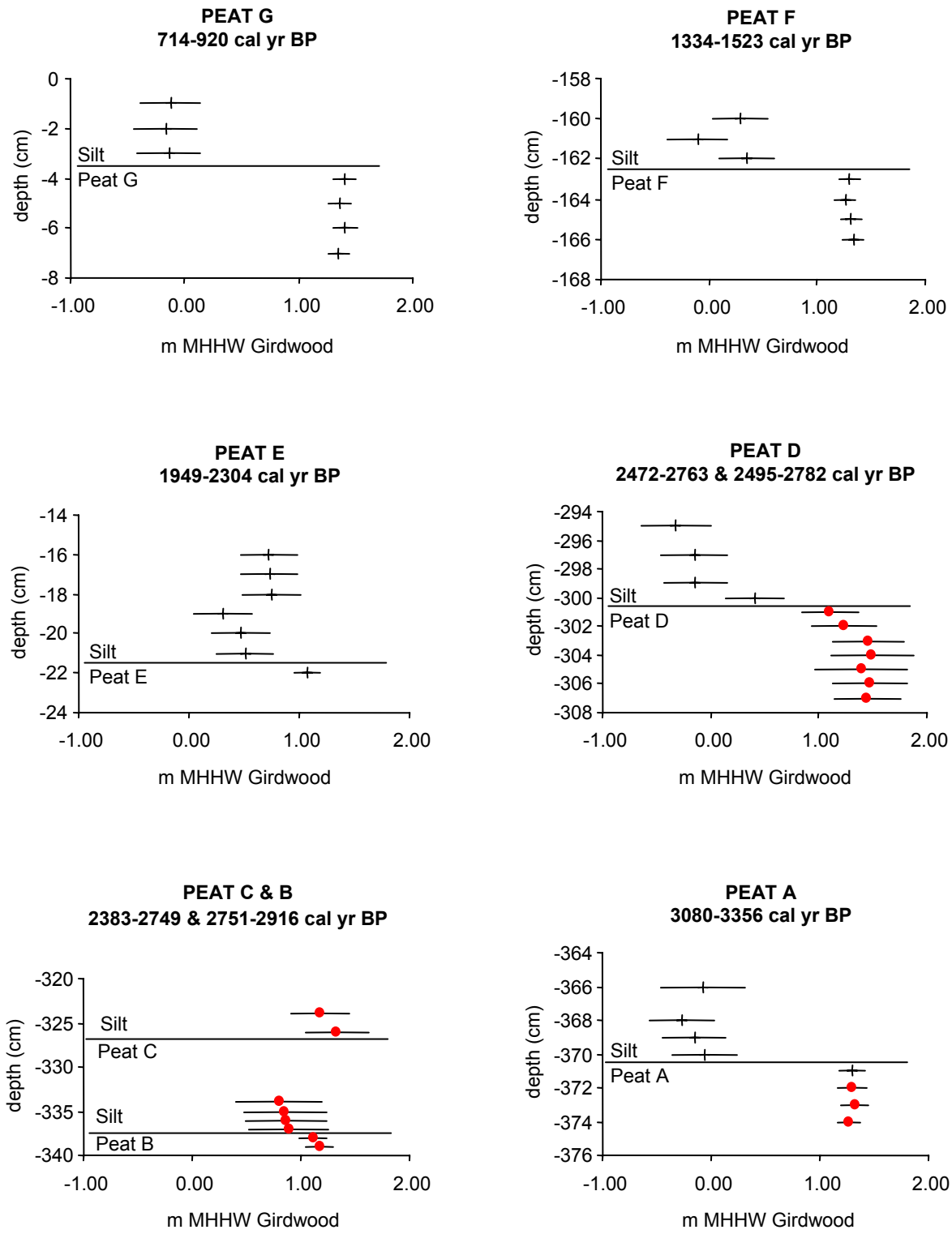

Figure 4.10

Elevation reconstructions for peat-silt couplets at Girdwood. Samples in red have 'poor' modern analogues.

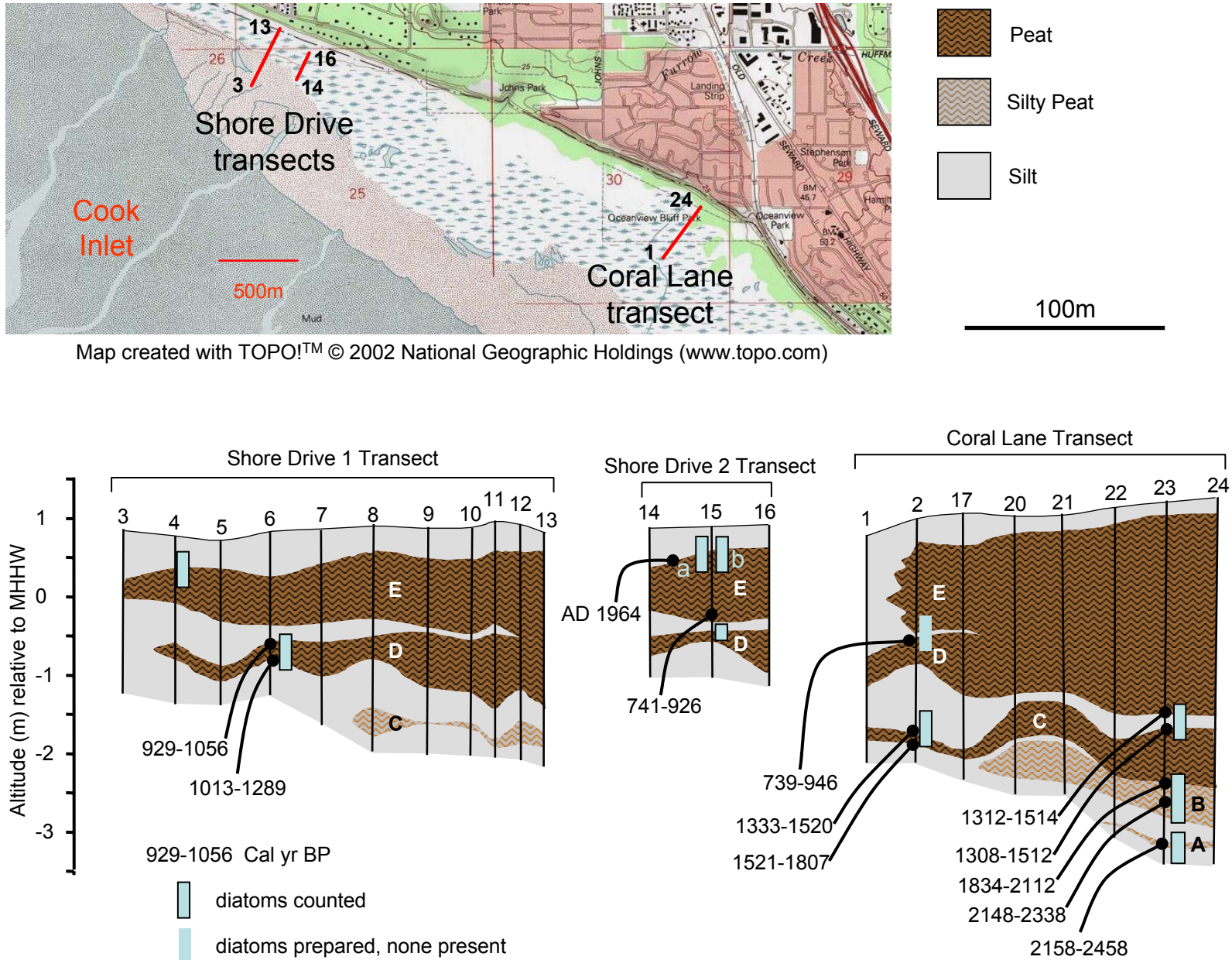

Figure 5.1
Location of sampling sites at Ocean View and sections showing the buried peat layers beneath the marsh surface.

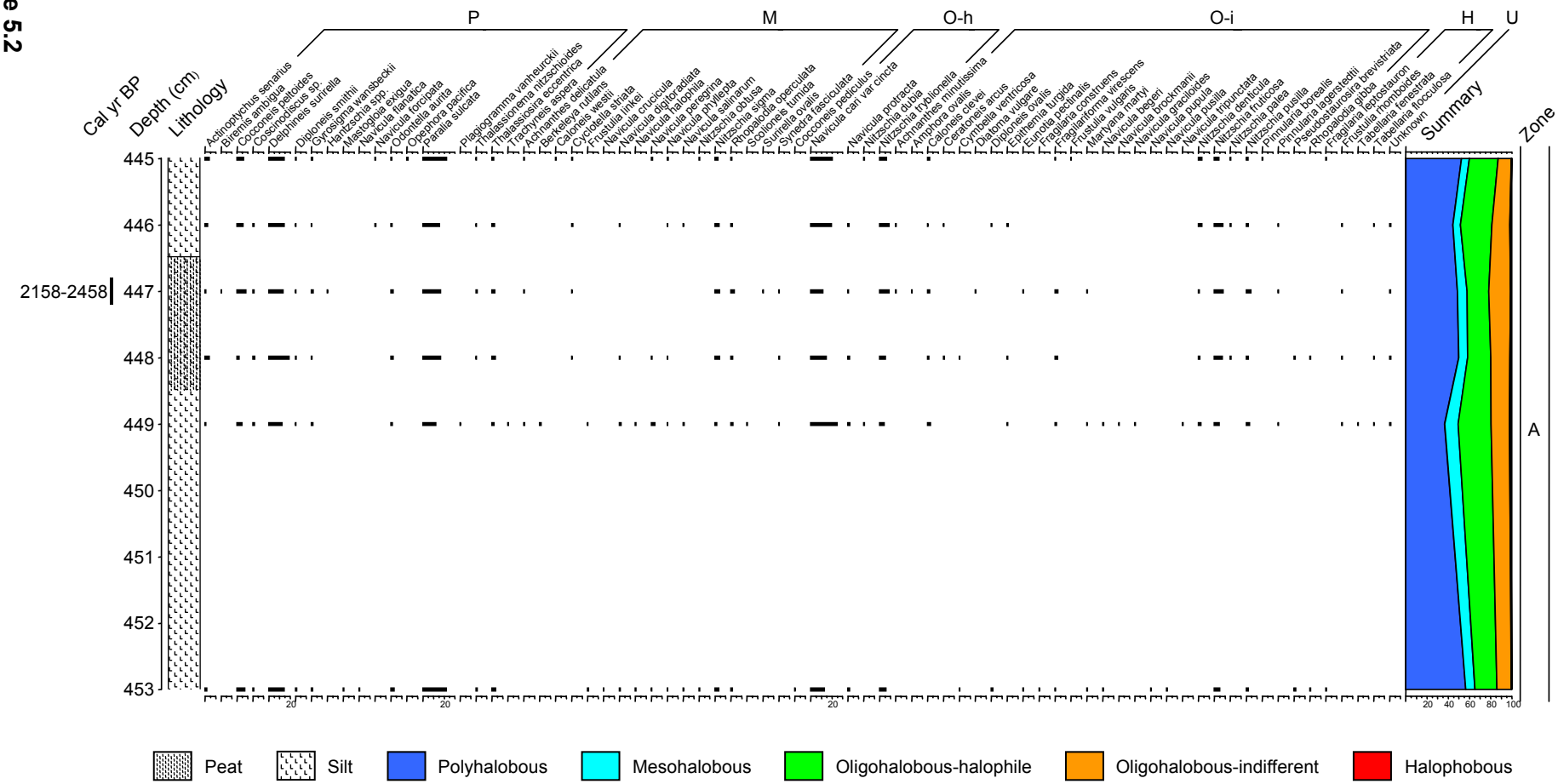

Figure 5.2
Bio-stratigraphy of unit A, OV-23 showing all diatoms counted. P: polyhalobous, M: mesohalobous, O-h: oligohalobous-halophile, O-i: oligohalobous-indifferent, H: halophobous diatom salinity groups ordered left to right in summary graph.

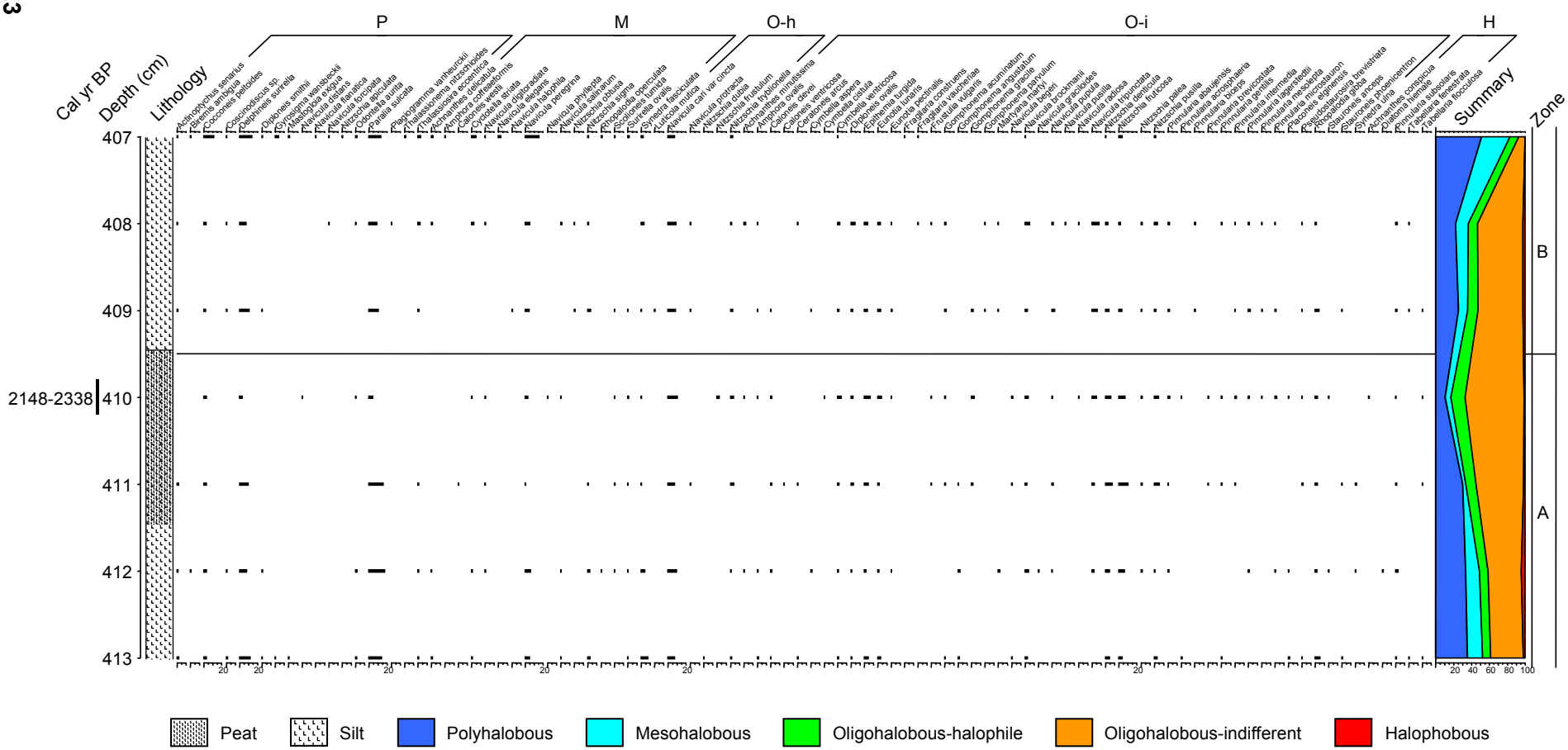

Figure 5.3
Bio-stratigraphy of unit B1, OV-23 showing all diatoms counted. P: polyhalobous, M: mesohalobous, O-h: oligohalobous-halophile, O-i: oligohalobous-indifferent, H: halophobous diatom salinity groups ordered left to right in summary graph.

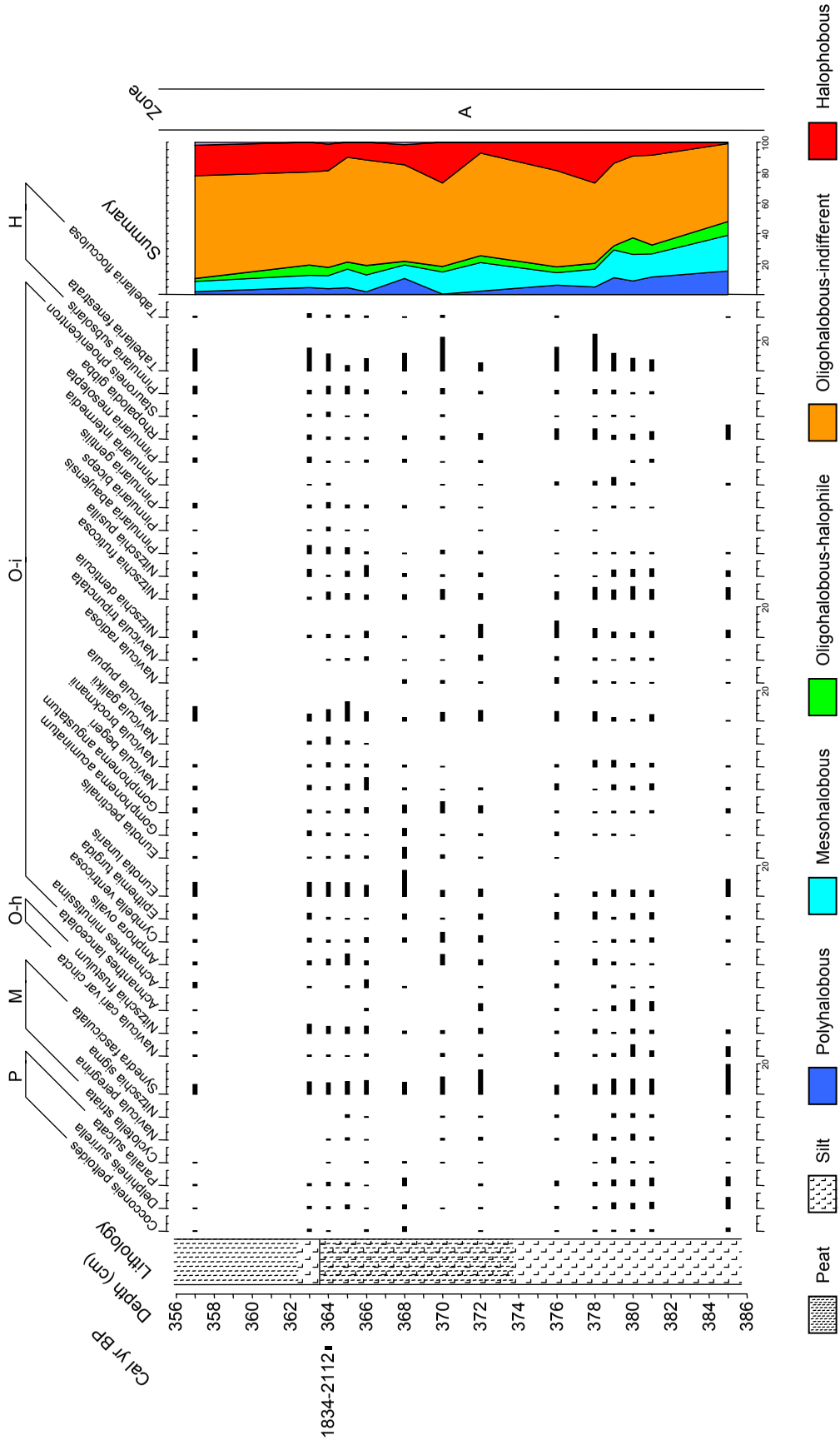

Figure 5.4
Bio-stratigraphy of unit B², OV-23 showing 2% total diatom valves counted. P: polyhalobous, M: mesohalobous, O-h: oligohalobous-halophile, O-i: oligohalobous-indifferent, H: halophobous diatom salinity groups ordered left to right in summary graph.

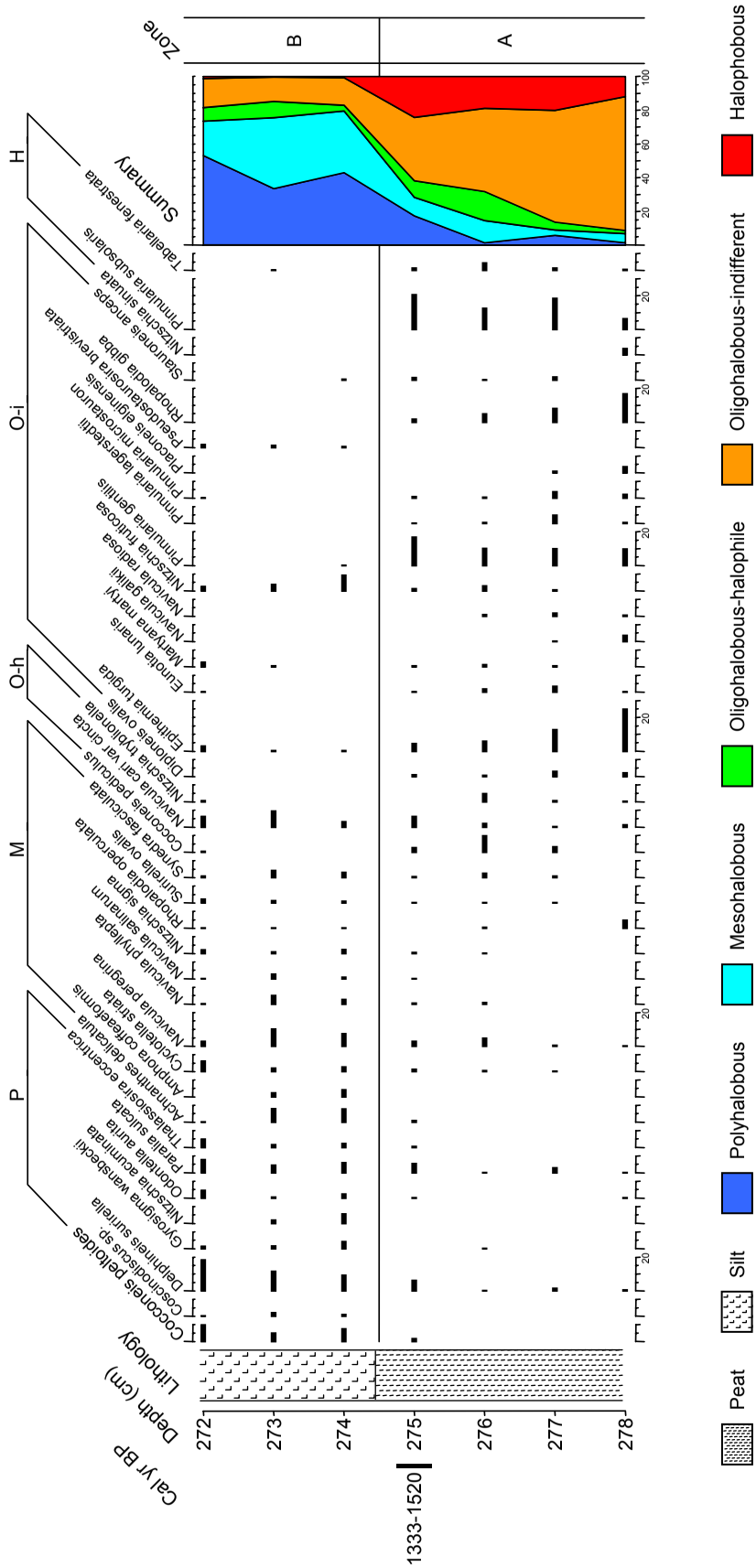

Figure 5.5

Bio-stratigraphy of peat C, OV-2 showing 2% total diatom valves counted. P: polyhalobous, M: mesohalobous, O-h: oligohalobous-halophile, O-i: oligohalobous-indifferent, H: halophobous diatom salinity groups ordered left to right in summary graph.

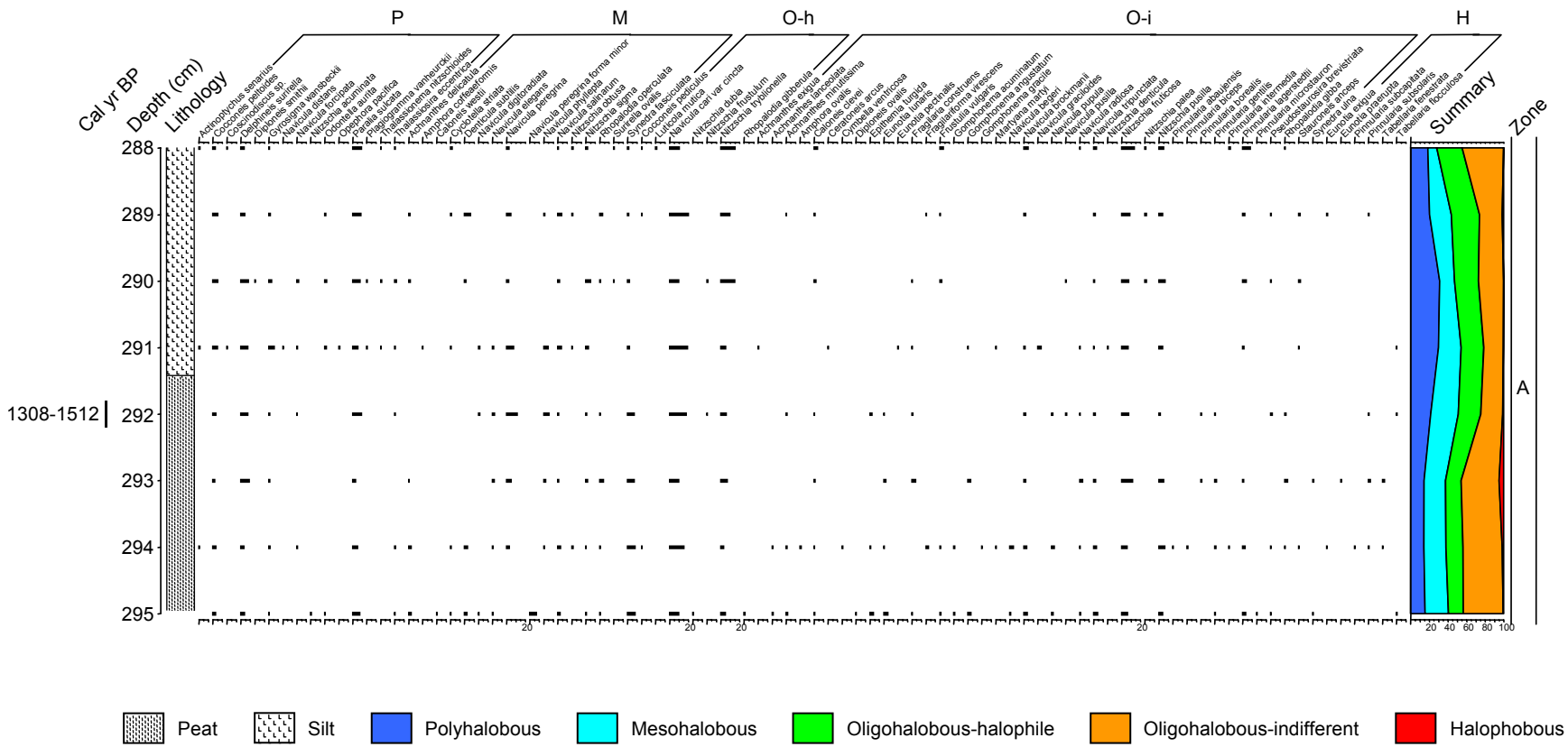

Figure 5.6

Bio-stratigraphy of peat C, OV-23 showing all diatoms counted. P: polyhalobous, M: mesohalobous, O-h: oligohalobous-halophile, O-i: oligohalobous-indifferent, H: halophobous diatom salinity groups ordered left to right in summary graph.

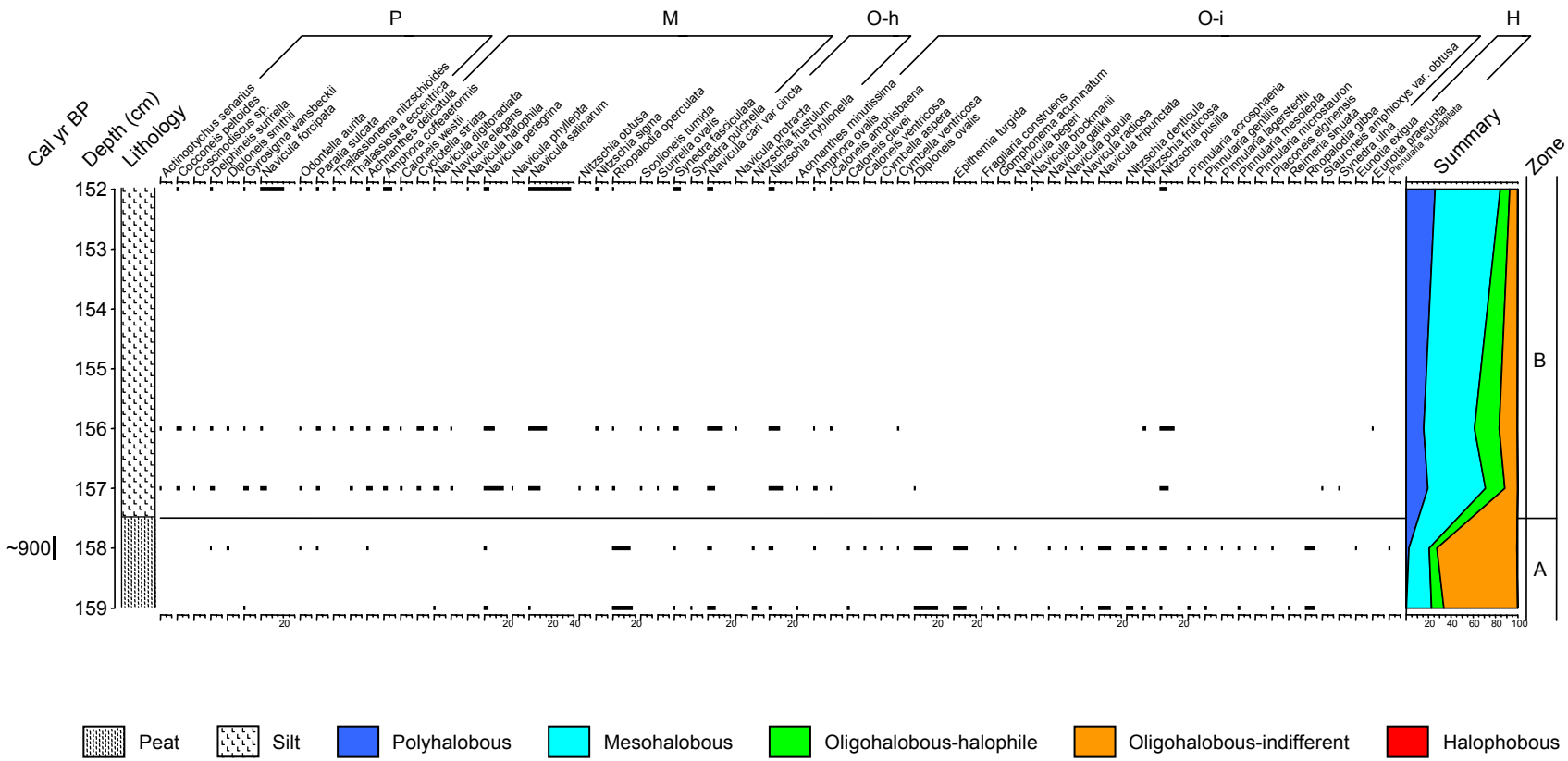

Figure 5.7
Bio-stratigraphy of peat D, OV-15 showing all diatoms counted. P: polyhalobous, M: mesohalobous, O-h: oligohalobous-halophile, O-i: oligohalobous-indifferent, H: halophobous diatom salinity groups ordered left to right in summary graph.

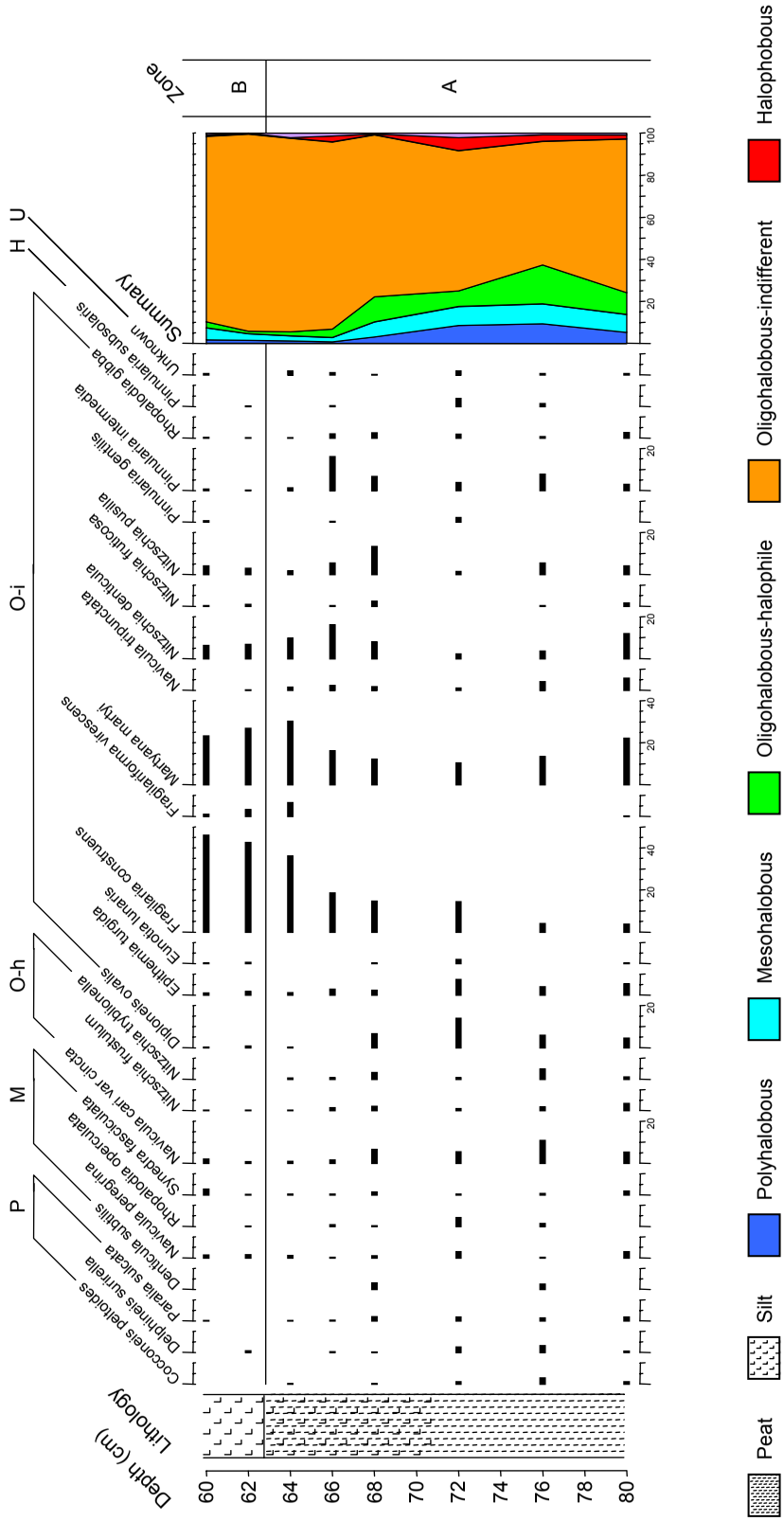

Figure 5.8
Bio-stratigraphy of peat E, OV-4 showing 2% total diatom valves counted. P: polyhalobous, M: mesohalobous, O-h: oligohalobous-halophile, O-i: oligohalobous-indifferent, H: halophobous diatom salinity groups ordered left to right in summary graph.

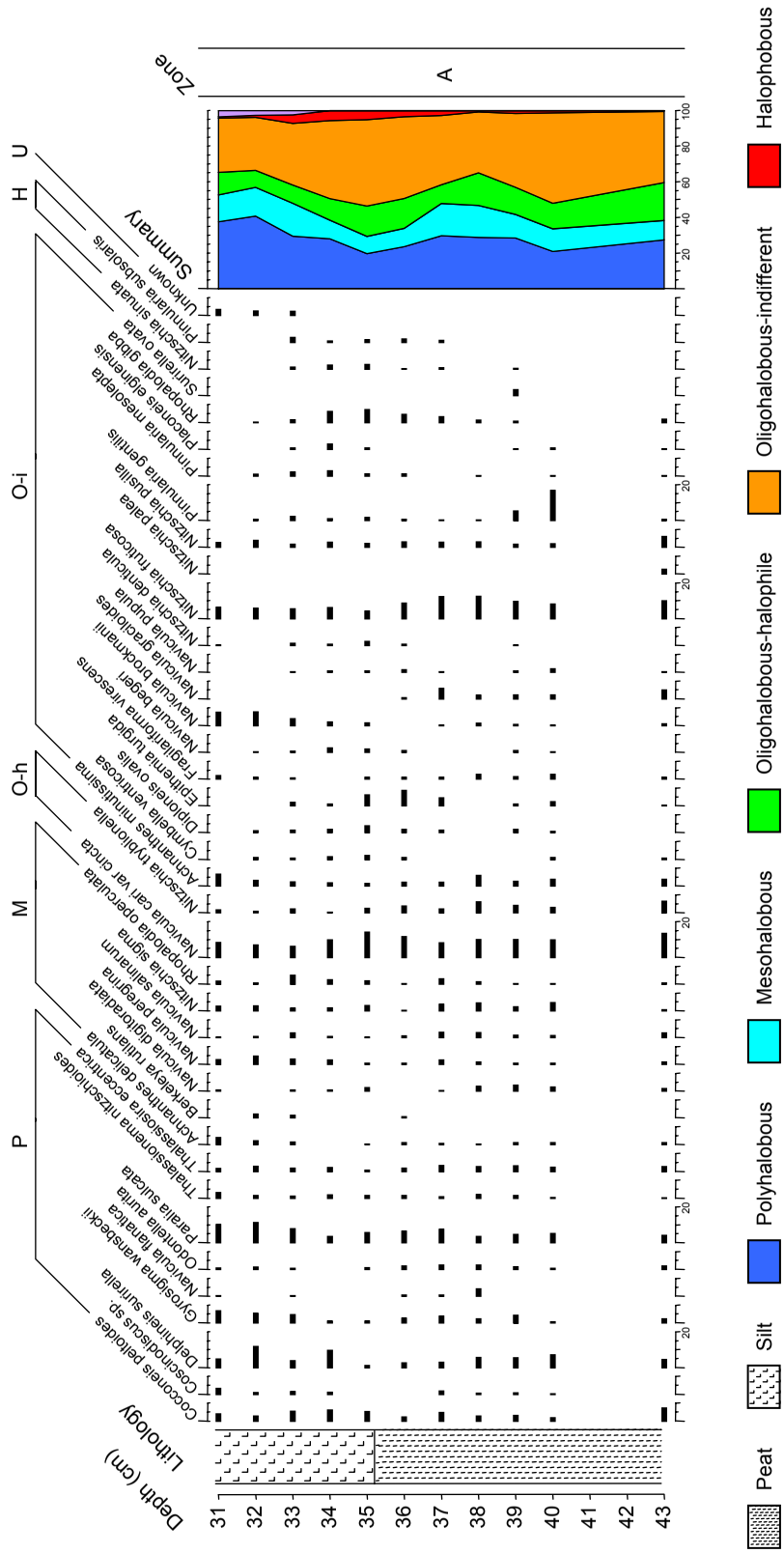

Figure 5.9
Bio-stratigraphy of peat E, OV-15b showing 2% total diatom valves counted. P: polyhalobous, M: mesohalobous, O-h: oligohalobous-halophile, O-i: oligohalobous-indifferent, H: halophobous diatom salinity groups ordered left to right in summary graph.

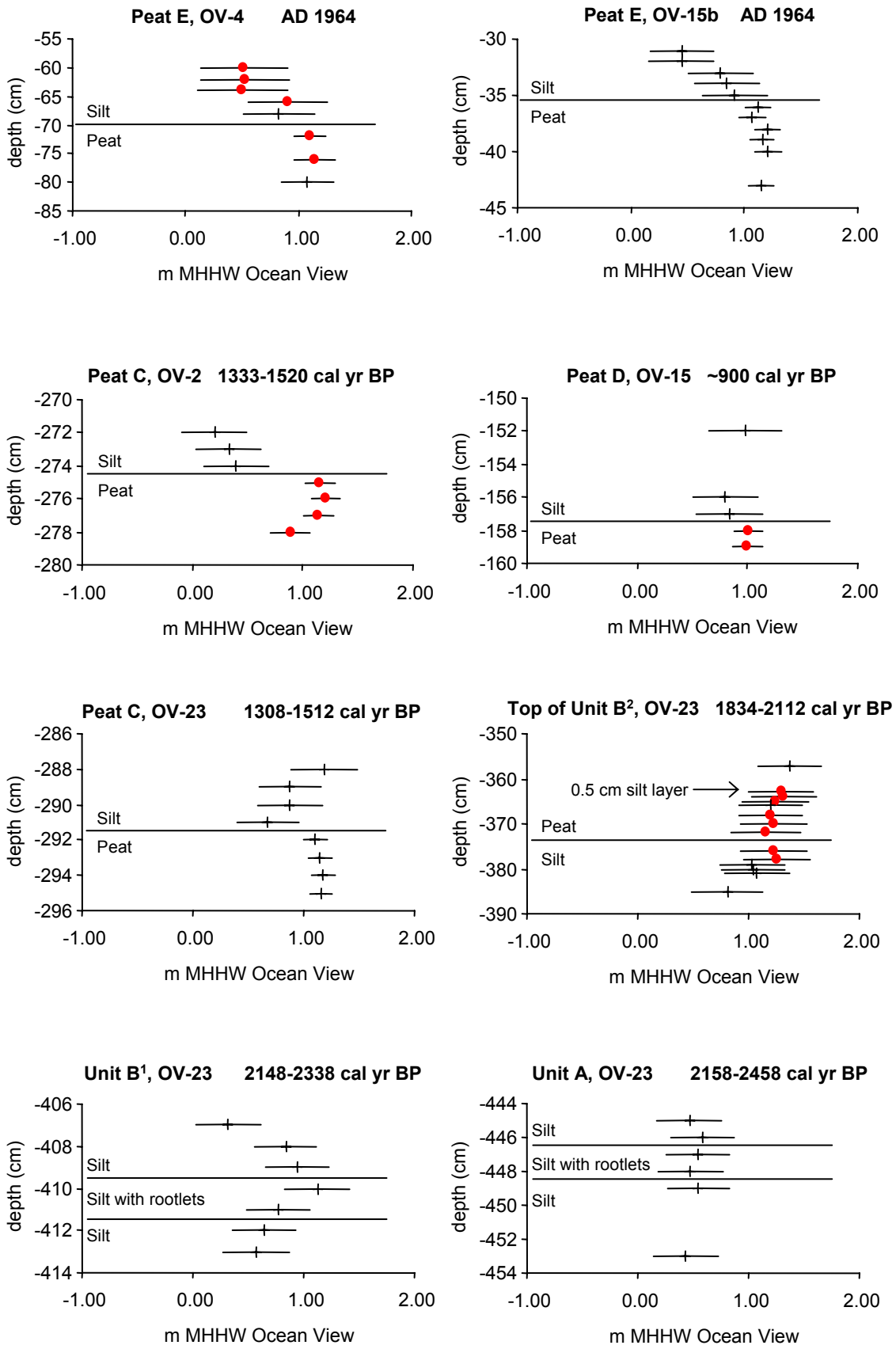

Figure 5.10

Elevation reconstructions for peat-silt couplets at Ocean View. Samples in red have 'poor' modern analogues.

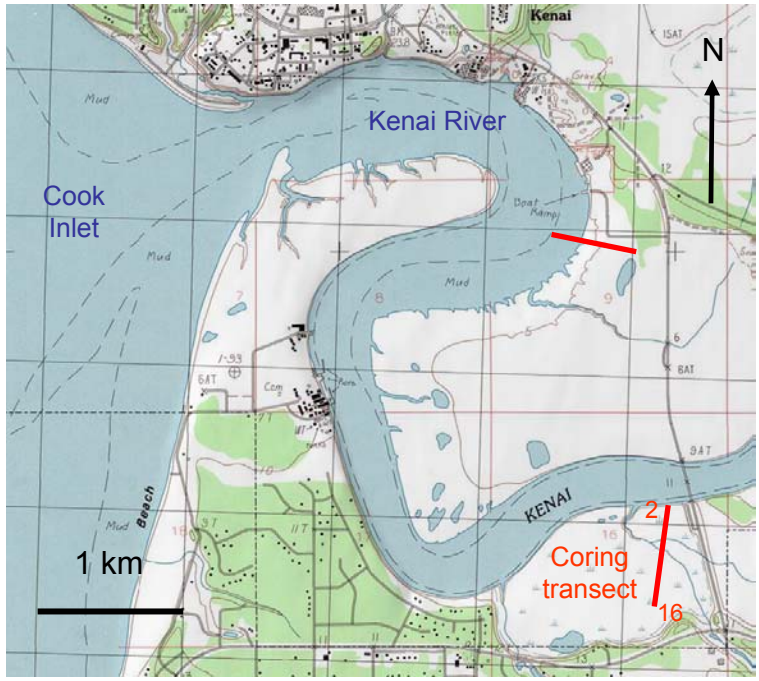

Map created with TOPO!™ © 2002 National Geographic Holdings (www.topo.com)

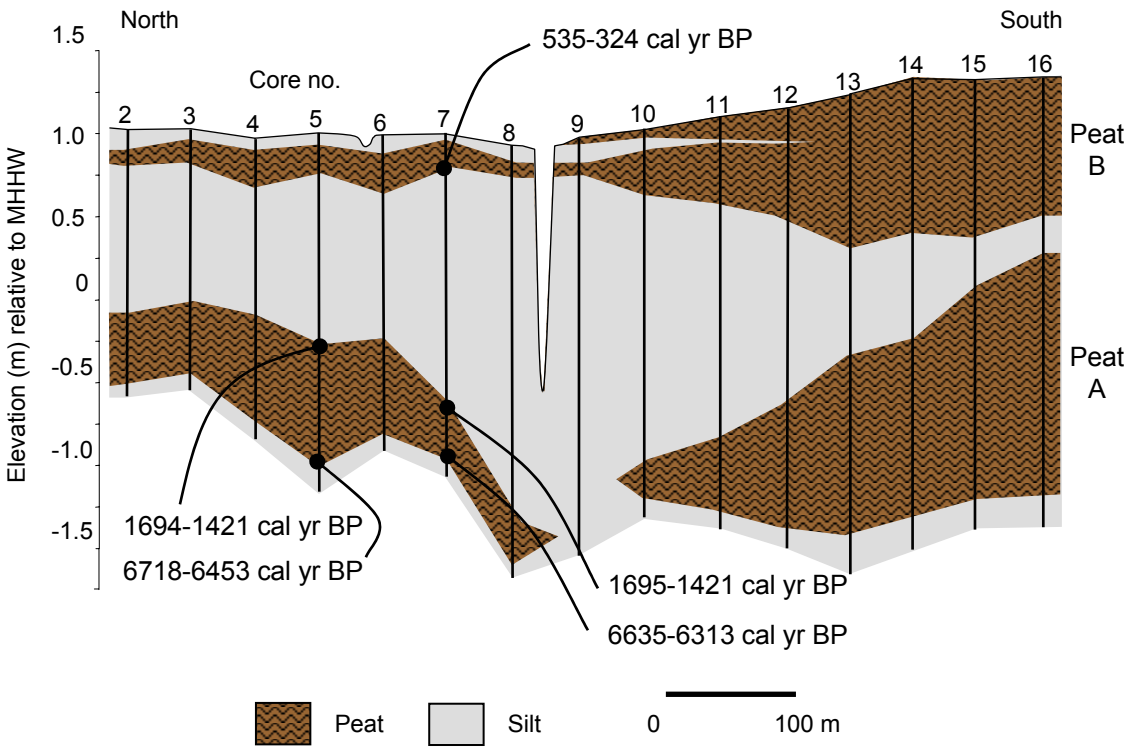

Figure 6.1
Location of sampling sites at Kenai and section showing the buried peat layers beneath the marsh surface

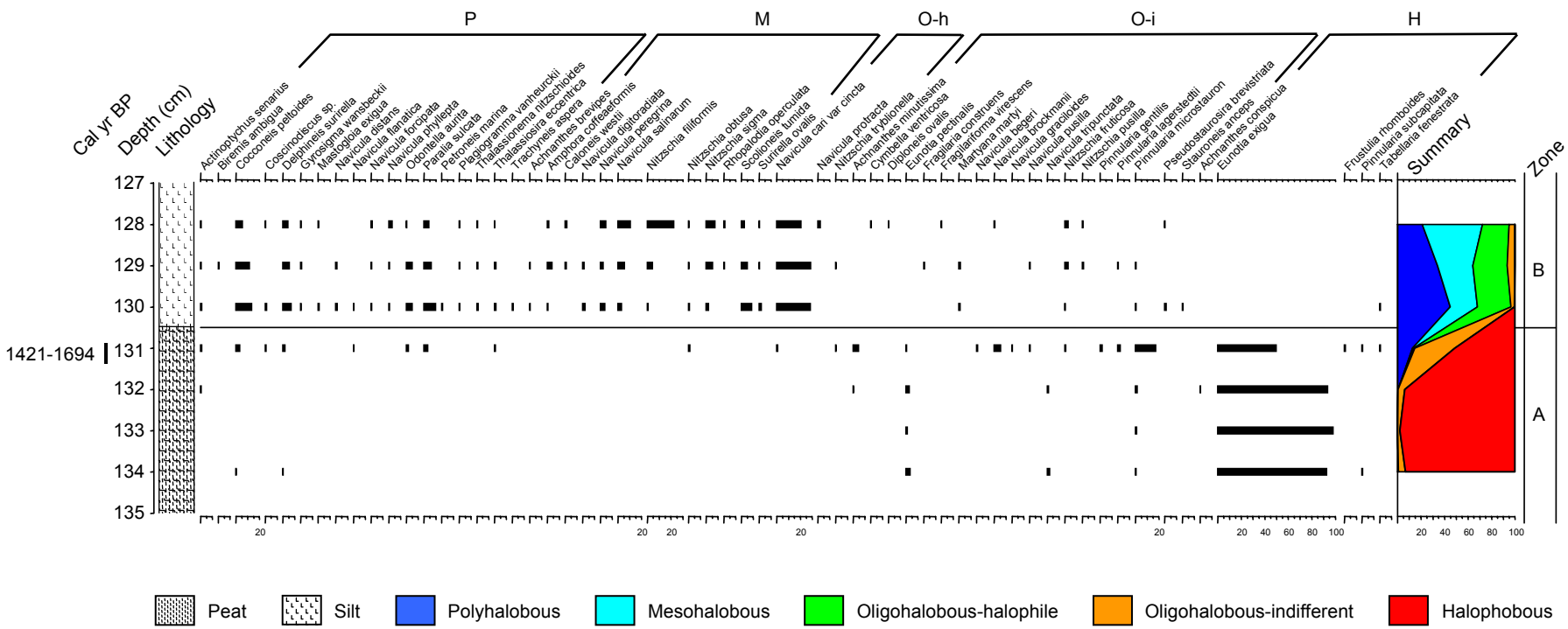

Figure 6.2
Bio-stratigraphy of peat A, KE-5 showing all diatoms counted. P: polyhalobous, M: mesohalobous, O-h: oligohalobous-halophile, O-i: oligohalobous-indifferent, H: halophobous diatom salinity groups ordered left to right in summary graph.

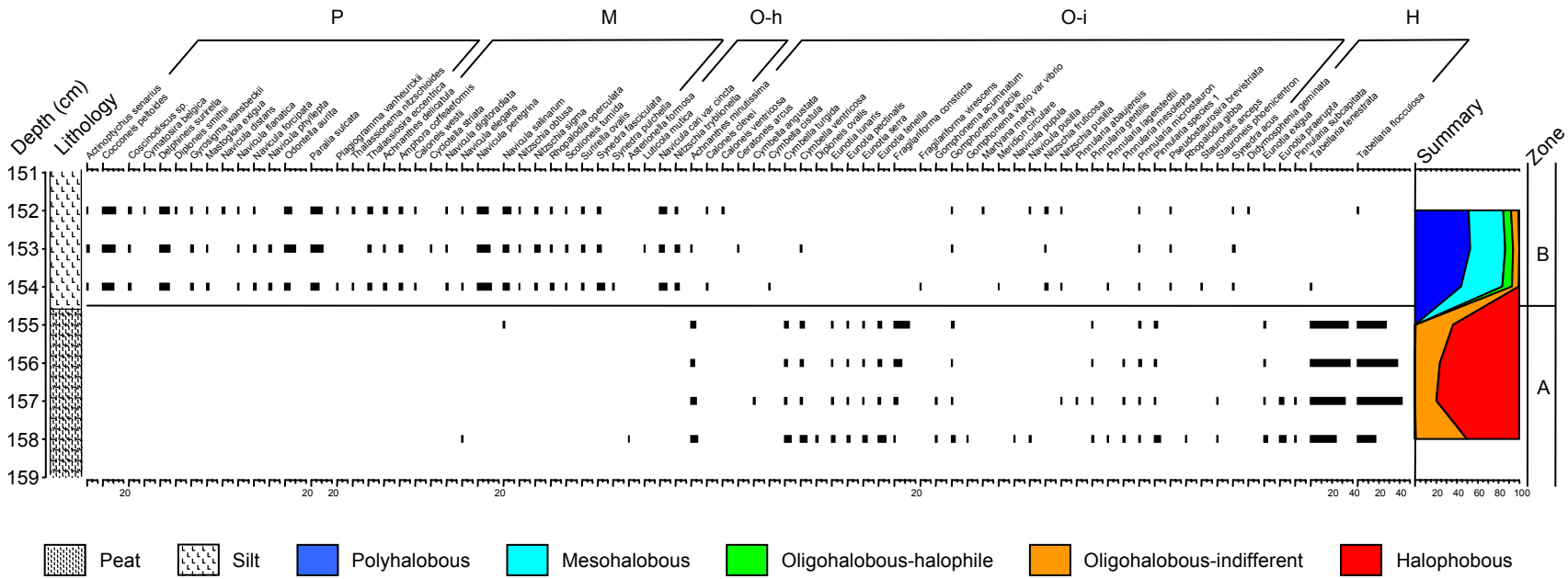

Figure 6.3
Bio-stratigraphy of peat A, KE-15 showing all diatoms counted. P: polyhalobous, M: mesohalobous, O-h: oligohalobous-halophile, O-i: oligohalobous-indifferent, H: halophobous diatom salinity groups ordered left to right in summary graph.

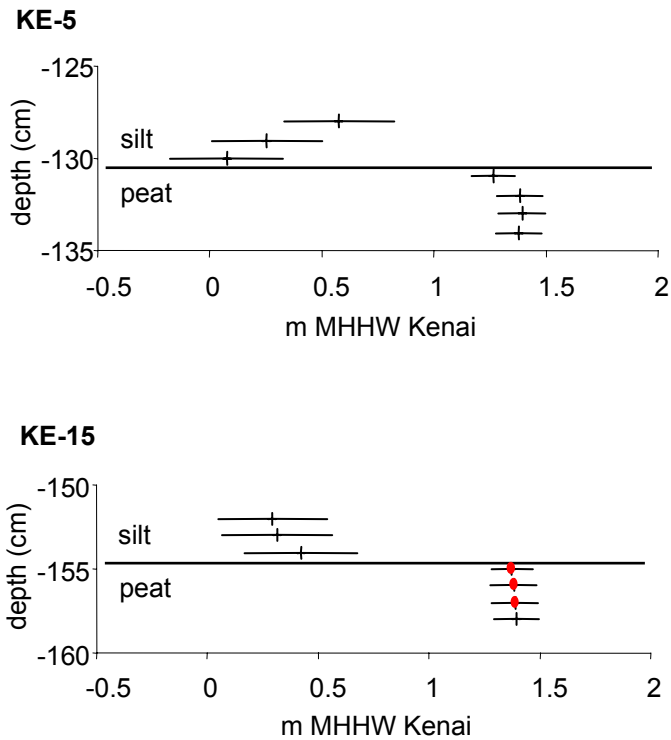

Figure 6.4
Elevation reconstructions for peat A, KE-5 and KE-15. Samples in red have 'poor' modern analogues.

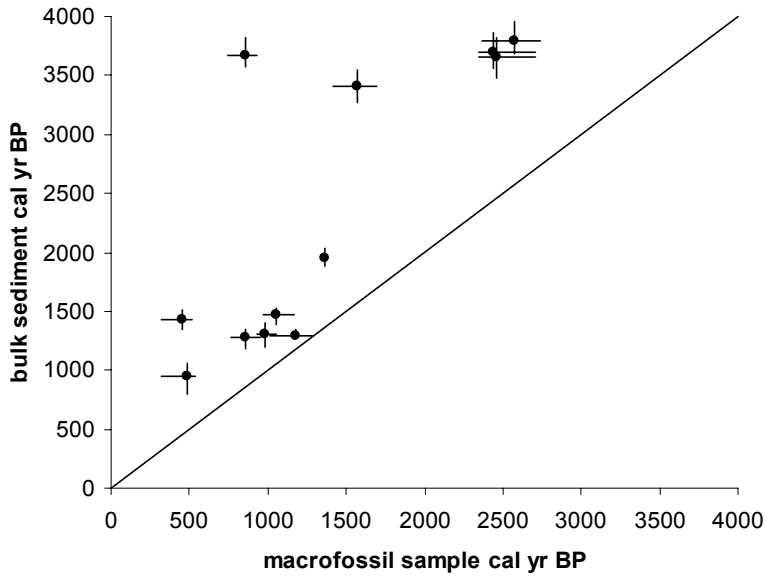

Figure 7.1
Comparison of AMS radiocarbon ages of paired samples from bulk peat and *in situ* macrofossils extracted from the peat (data from Hamilton, 2003 and this report), plotted as median calibrated ages with 2σ error range.

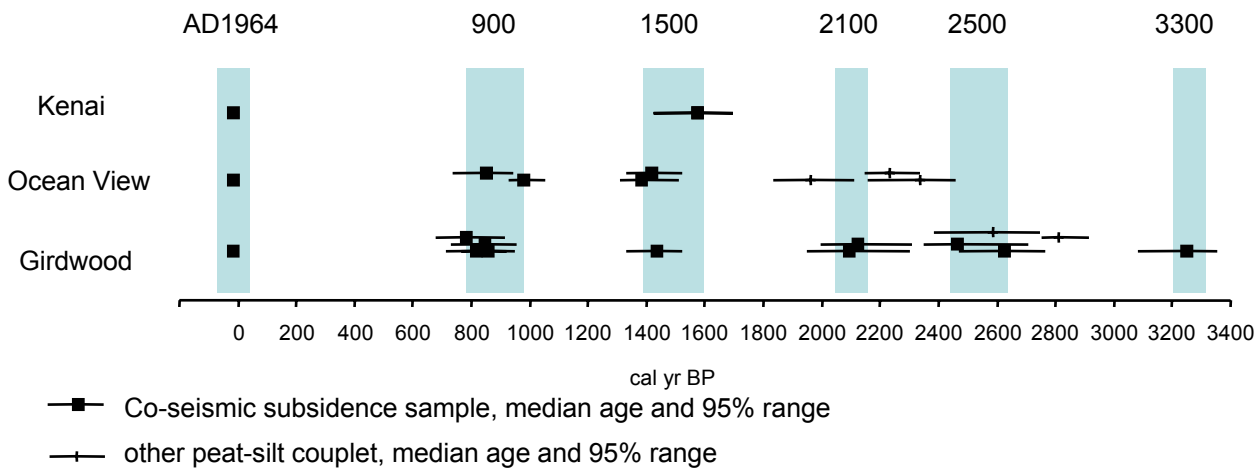

Figure 7.2
Ages of earthquakes recorded at three sites around the Cook Inlet. Shaded boxes show (1) within-site correlations established from supporting lithostratigraphy of samples indicating coseismic submergence and (2) between-site correlations based on sample ages. Samples from other peat-silt couplets are ages from the tops of separate peat or silt-peat horizons, two at Girdwood and three at Ocean View, where diatom data show no evidence for rapid submergence.

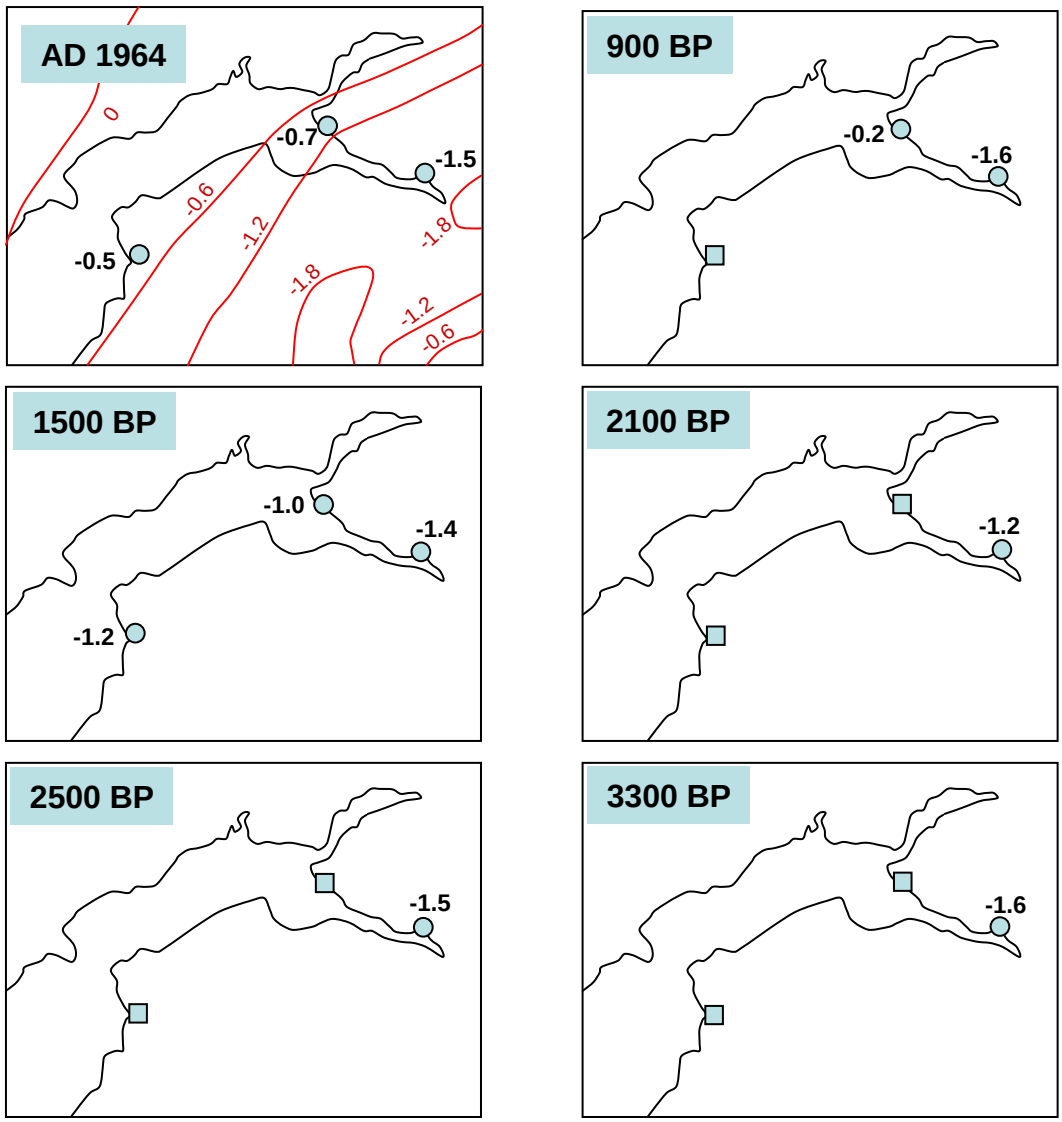

Stratigraphic evidence for coseismic deformation (m) quantified from diatom transfer function reconstructions

No conclusive evidence for coseismic deformation

Contours of deformation (m) from observations after AD 1964 earthquake (after Plafker, 1969)

Figure 7.3
Co-seismic subsidence during six great earthquakes at three sites around upper Cook Inlet

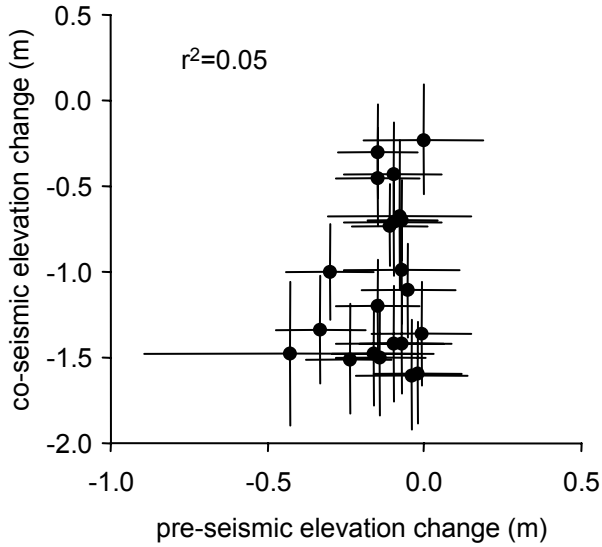

Figure 7.4
Comparison of pre-seismic and co-seismic elevation change (data from Table 7.1).